GhostParser: A highly scalable phylogenomic approach for the identification of ghost introgression

Ethan R. Tolman[1,2*], Anton Suvorov[1*]

[1]Department of Biological Sciences, Virginia Tech, Blacksburg, VA
[2]Department of Invertebrate Zoology, American Museum of Natural History, New York, NY
*Corresponding authors (etolman@vt.edu, asu@vt.edu)

Abstract

A growing body of empirical research shows that interspecific gene flow is a widespread biological force that shapes evolutionary histories across the Tree of Life. Computational approaches designed to detect introgression either employ full likelihood, including Bayesian, frameworks to directly estimate phylogenetic networks or utilize summary statistics derived directly from locus sequence alignments or estimated gene trees to map gene flow events onto the species tree. Many current methods currently have major shortcomings. The computationally scalable summary statistics and pseudo-likelihood-based techniques may provide erroneous results in the presence of so-called “ghost” introgression and rate variation between lineages. On the other hand, full likelihood methods are more accurate, but are not computationally tractable for large phylogenomic datasets. Here, we develop a novel summary statistic, based on tree heights of different gene tree topologies to reliably distinguish between sampled and ghost introgression events. We implemented this approach in the publicly accessible bioinformatic pipeline “GhostParser”. We demonstrate that GhostParser can accurately distinguish between scenarios of sampled and ghost introgression, even in the presence of rate variation between lineages. Our methodology generally concurs in accuracy with the full likelihood software Bayesian Phylogenetics and Phylogeography (BPP) on empirical datasets, and outperforms BPP in our simulation conditions, both in a small fraction of the computational time. We show that GhostParser is a scalable tool for the identification of different introgression patterns in phylogenomic datasets.

Keywords: Systematics, Bioinformatics, Gene flow, Multispecies coalescent, Tree height

Introduction

A major shift in phylogenomics has been the realization that the evolutionary relationships oftentimes cannot be most accurately described by a binary tree model. Introgression is a source of novel genetic variation, which may be deleterious, adaptive or neutral and can cause the involved species or populations to share both genotypes and phenotypes (Whitney et al. 2006; Pardo-Diaz et al. 2012; Huerta-Sánchez et al. 2014; Bastide et al. 2018; Jones et al. 2018; Taylor and Larson 2019; Gibson et al. 2021; Hibbins and Hahn 2021). In a multi-locus dataset, introgression will produce an excess of loci supporting the same discordant history—that is, a higher proportion of gene trees will share an alternative topology that does not match the species tree. Such a signature of introgression has been identified in many lineages across the Tree of Life including vascular plants (Stull et al. 2023), mammals (Hallström and Janke 2010; Kumar et al. 2017; Teixeira and Cooper 2019; Gokcumen 2020; McArthur et al. 2021; Koller et al. 2022), birds (Singhal et al. 2021), fishes (Bernal et al. 2017; Qian et al. 2023), and arthropods (Leduc-Robert and Maddison 2018; Suvorov et al. 2022A,B; Thawornwattana et al. 2023). Indeed, as many as 10% of extant fauna and 25% of extant flora are estimated to be involved in introgression with other species (Mallet 2005). In each of these systems, and in all other clades where introgression has occurred, evolutionary history is better described as a phylogenetic network, than as a strictly bifurcating phylogenetic tree (Huson and Bryant 2006).

While many classical studies of introgression employ a "sampled introgression" model whereby gene flow is assumed to have involved two sampled lineages (Green et al. 2010; Edelman et al. 2019; Suvorov, et al. 2022A,B), this model does not fit every species network (Tricou, et al. 2022A,B). In many systems a "ghost introgression" model in which gene flow occurs from an unsampled lineage to a sampled lineage is more appropriate (Zhang et al. 2019; Ottenburghs 2020a; Chang et al. 2023; Pang and Zhang 2024; Zhang et al. 2024). Both models of introgression will result in an excess of loci supporting an alternative evolutionary history than

a recovered species tree, and can also pose challenges for species tree estimation (Tricou et al., 2022A,B, Pang and Zhang 2023,2024). Distinguishing between models of ghost and sampled introgression is an important consideration in evolutionary biology, as an incorrectly applied introgression model can lead to erroneous conclusions regarding adaptation, speciation, and even the morphology of extinct lineages (Ottenburghs 2020b).

Identifying introgression

The inference of introgression from phylogenomic datasets can be compromised by various factors. One of such factors is the among-lineage rate variation that increases branch length heterogeneity obscuring the signal of actual introgression in tests that utilize branch length, and creating a false positive signal of introgression between lineages in a multi-species network by making slower evolving lineages appear to have introgressed (Frankel and Ané 2023; Koppetsch et al. 2024).

The vast majority of current computational approaches designed to estimate reticulate evolution either utilize summary statistics derived from multiple sequence alignments (MSA) or gene trees to map events onto an estimated species tree (Edelman et al. 2019; Hahn and Hibbins 2019; Malinsky et al. 2021; Suvorov,, et al. 2022A), directly infer a phylogenetic network in either a pseudo-likelihood (Solís-Lemus et al. 2017; Allman et al. 2019) or in full-likelihood (including Bayesian) frameworks (Hey et al. 2018; Wen and Nakhleh 2018; Zhang et al. 2018; Flouri et al. 2020b, Pang and Zhang 2024). These current methods offer a major tradeoff in accuracy and computational feasibility (Hibbins and Hahn 2022; Pang and Zhang 2024; Pfeifer et al. 2024).

Full likelihood approaches

Full likelihood methods that leverage multilocus sequence data directly, consider the joint distribution of coalescent times and gene-tree topologies to infer phylogenetic networks (Jiao et al. 2021). The full likelihood approach implemented in Bayesian Phylogenetics and Phylogeography (BPP) program (Flouri et al. 2020a) is considered to be the most accurate tool

to identify introgression in multi-locus datasets. Furthermore, BPP provides the most accurate framework for distinguishing between ghost and sampled introgression models based upon testing in simulated and empirical datasets (Pang and Zhang 2024). BPP considers the joint probability distribution of gene-tree topologies and coalescent times under sampled and ghost introgression, using the foundational multi species coalescent with introgression (MSci) model (Flouri et al. 2020a). The marginal likelihoods of ghost, sampled inflow and outflow introgression models are compared for a given dataset to select the best fitting model, and identify gene flow involving sampled and ghost lineages. This technique has been demonstrated to be robust in the presence of between lineage-rate variation (Pang and Zhang 2024). However, even though BPP is potentially more scalable than other implementations of full likelihood approaches to identify introgression (Hey et al. 2018; Wen and Nakhleh 2018; Zhang et al. 2018; Flouri et al. 2020b; Pfeifer et al. 2024), computational resources remain a major barrier in its implementation. For instance, BPP, will require approximately 6 hours of real compute time to compare three different introgression scenarios for one species triplet with 1000 loci of 1000 basepairs each (Pang and Zhang 2024), making it unscalable for large taxon and/or locus sampling.

Pseudo-likelihood approaches for detecting introgression

Alternatively, pseudo-likelihood methodologies which estimate a phylogenetic network from gene trees are moderately less computationally intensive than the full likelihood approaches (Yu et al. 2014a). These methods estimate a phylogenetic network utilizing gene tree topologies within a (pseudo-)likelihood or distance-based framework (Yu et al. 2014a; Solís-Lemus et al. 2017; Pang and Zhang 2024). They all evaluate the pseudo-likelihood functions of different phylogenetic networks in order to identify the one that best explains the observed gene tree discordance under the multispecies network coalescent (MSNC) model. Implementations include InferNetwork_ML and InferNetwork_MPL from PhyloNet (Yu et al. 2014b; Yu and Nakhleh 2015), NANUQ from MSCquartets (Allman et al. 2019) and SNaQ from PhyloNetworks (Solís-Lemus and Ané 2016). Although, these pseudo-likelihood approaches are capable of differentiating

between ghost and sampled introgression, they are sensitive to model misspecification (Pang and Zhang 2024) and can also falsely infer introgression between lineages when rate variation between lineages is present (Frankel and Ané 2023).

Heuristic approaches for detecting introgression

In comparison with full- and pseudo-likelihood approaches, heuristic based techniques for detecting introgression are highly computationally scalable, and can analyze hundreds of triplets or quartets with thousands of loci in a matter of minutes. Despite such appealing scalability these approaches are oftentimes less accurate and incapable of identifying ghost introgression. Typically, heuristic approaches rely on various summary statistics which can be obtained from either MSAs or gene trees. First, site pattern-based methods (e.g. the D-statistic (Green et al. 2010; Zheng and Janke 2018), HyDe (Blischak et al. 2018), and Dfoil (Pease and Hahn 2015)) compute certain asymmetries in pattern frequencies, that can be indicative of introgression. Second, gene tree topology count-based techniques (e.g. the Discordant Counts Test (Suvorov, et al. 2022A)) assess species tree-gene tree heterogeneity. Finally, branch length-based approaches (e.g. the Branch Length Test (Suvorov et al. 2022A), D3 (Hahn and Hibbins 2019), and QuiBL (Edelman et al. 2019)) utilize branch length distributional differences. Typically, the counts or branch lengths in the most abundant discordant topology are compared to those in the least abundant discordant topology. These methods can all flag possible gene flow patterns across an input species tree in a matter of minutes to hours in a large multilocus dataset, but they cannot distinguish between ghost and sampled introgression accurately, if it all, and oftentimes erroneously identify ghost introgression as sampled (Tricou et al., 2022A,B; Pang and Zhang 2024). Heuristic tests can also exhibit elevated rates of false positives for sampled introgression in the presence of between-species rate variation, nevertheless topology count-based methods are less susceptible to producing false positives than methods, which rely on branch lengths (Frankel and Ané 2023; Koppetsch et al. 2024).

A new approach for distinguishing ghost and sampled introgression

Here, we developed a new heuristic-based strategy to detect sampled and ghost introgression that relies on a simple gene tree summary statistic based on the averaged tree height. Additionally, we provide theoretical justification for its usage and show how it reduces biases associated with heterogeneity of rate variation among lineages. Our approach can correctly identify ghost introgression in simulated datasets with high accuracy, specificity and sensitivity. This method concurs with BPP (the only introgression detection software which is currently known to be unaffected by rate variation and can accurately distinguish between sampled and ghost introgression, but is limited in its application by the computational time necessary to run it) in empirical datasets where full-likelihood and other summary-statistics based methods failed. Our approach also differentiates between various introgression models with higher accuracy than BPP in our simulated scenarios. We use our technique to revisit several hypothesized instances of introgression, and demonstrate that some of these “classical” reticulation events are likely instances of ghost introgression. Our approach is implemented in the bioinformatic software GhostParser, which will be a useful tool for evolutionary biologists to disentangle sampled and ghost introgression in a scalable manner.

Materials and Methods

Conceptual framework

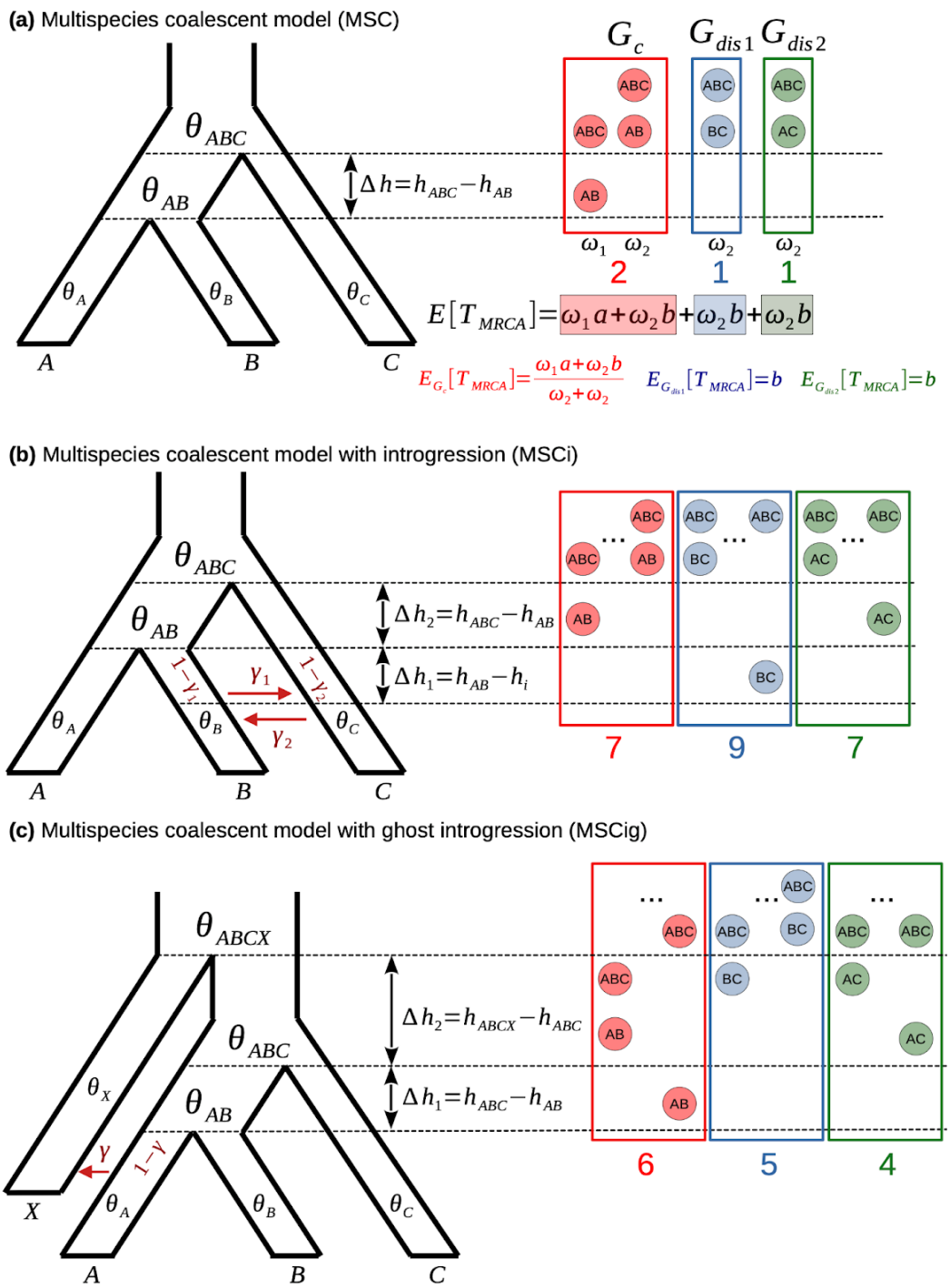

Fig. 1 Parametrizations of GhostParser models: a) Multispecies coalescent (MSC) model of three species A, B and C with the corresponding population parameters $\Theta = (\theta_A, \theta_B, \theta_C, \theta_{AB}, \theta_{ABC})$ placed within the species tree topology $((A,B),C)$. The arrow between dashed lines represents the duration Δh of the branch calculated as the difference between divergence times h_{AB} and h_{ABC}. The circles on the right denote the lineages (i.e. AB and ABC) and populations in which the first and second coalescence events of each triplet occur for concordant $G_c = ((A,B),C)$ as well as discordant $G_{dis1} = ((B,C),A)$ and $G_{dis2} = ((A,C),B)$ topologies grouped by red, blue and green rectangles, respectively. The ω parameters represent probabilities at which such coalescence event configurations occur. The numbers below each rectangle show the number of ω parameters for concordant and two discordant topologies (see

Appendix for more details). $\mathbb{E}[T_{MRCA}]$ represents the expected gene tree height that can be viewed as mixture weighted by ω parameters, where a and b denote tree height for a specific gene tree. $\mathbb{E}_{G_c}[T_{MRCA}]$, $\mathbb{E}_{G_{dis1}}[T_{MRCA}]$, and $\mathbb{E}_{G_{dis2}}[T_{MRCA}]$ represent normalized expected values for gene tree heights of concordant and discordant topologies, respectively. **b)** Multispecies coalescent model with bidirectional introgression (MSCi) between non-sister species B and C. Red arrows indicate inflow and outflow introgression, with the introgression ("inheritance") probabilities, γ_1 and γ_2, respectively. **c)** Multispecies coalescent model with ghost introgression between the extinct (unsampled) lineage X and extant species A. In this case only outflow introgression with probability γ is considered.

Here, we provide theoretical foundations for our triplet-based statistical tests that will be used to estimate introgression under different multispecies coalescent models. The tests of introgression for our method primarily rely on the disparity of gene tree frequencies as well as their expected heights, i.e. T_{MRCA}. For all the models considered here we establish two fundamental assumptions: (i) evolutionary history between taxa is known in a form of a phylogenetic tree and (ii) only one gene copy is sampled from the extant taxa.

For the first null model (**Fig 1a**), which is a traditional multispecies coalescent (MSC) framework (Rannala and Yang 2003), we assume that there are three species, A, B and C that are related by the species tree topology $S = ((A, B), C)$. Further, we specify divergence times $H = (h_{AB}, h_{ABC})$ and let $\Theta = (\theta_A, \theta_B, \theta_C, \theta_{AB}, \theta_{ABC})$ be the population-scaled mutation rate, i.e. $\theta = 4N_e\mu$ (Ewens 2004), where N_e and μ are effective population size and mutation rate, respectively. Both H and Θ are expressed in the expected number of mutations per site. Additionally, we define the probability (Rosenberg 2002) that two lineages (the number of lineages denoted as the superscript of P) do *not* coalesce (denoted as 0 in the subscript of P) in a population (e.g AB) as:

$$P^{(2)}_{0,AB} = e^{-\frac{2}{\theta_{AB}}(h_{ABC}-h_{AB})} = e^{-\frac{2}{\theta_{AB}}\Delta h}.$$

Thus, under the standard multispecies coalescent model (Pamilo and Nei 1988; Maddison 1997; Hudson 2002), the probability of concordant $G_c = ((A, B), C)$ and discordant $G_{dis1} = ((B, C), A)$

and $G_{dis2} = ((A, C), B)$ gene tree topologies are:

$$P(G_c) = 1 - \frac{2}{3}P^{(2)}{}_{0,AB}\ ,\ P(G_{dis1}) = \frac{1}{3}P^{(2)}{}_{0,AB}\ ,\ P(G_{dis2}) = \frac{1}{3}P^{(2)}{}_{0,AB}\ .$$

Obviously, under MSC the probabilities of concordant topology is larger than any of discordant topologies, i.e. $P(G_c) > P(G_{dis1})$ or $P(G_{dis2})$. Additionally, the probabilities of discordant topologies are equal, i.e. $P(G_{dis1}) = P(G_{dis2})$. These probability comparisons for our null model provide a foundation for topology frequency tests (see below; Suvorov, et al. 2022A).

Now we consider the expected tree height T_{MRCA} for a gene tree in a single population with a constant N_e, which can be expressed as $\mathbb{E}[T_{MRCA}] = \mathbb{E}[T_2 + T_3 + . . . + T_{n-1} + T_n]$ where T is the waiting time until next coalescence and its subscript denotes the total number of lineages k before a coalescence event that will reduce them to $k - 1$ (Wakeley 2009). The distribution of waiting time t_j until a coalescent event exhibits an exponential density:

$$f(T = t_i) = \frac{i(i-2)}{2}\frac{2}{\theta}e^{-\frac{i(i-2)}{2}\frac{2}{\theta}t_i},$$

with the $\mathbb{E}[T_i] = \frac{\theta}{i(i-2)}$ (Wakeley 2009).

In MSC, however, in order to compute $\mathbb{E}[T_{MRCA}]$ we need to account for the probability ω of each gene tree and population parameters that can vary among species tree's branches (see Appendix for more details). Thus, the expected gene tree height under the MSC model can be viewed as a weighted mixture. Define $a = \mathbb{E}_{\theta_{ABC}}[h_{ABC} + T_2] = h_{ABC} + \mathbb{E}_{\theta_{ABC}}[T_2]$ and $b = \mathbb{E}_{\theta_{ABC}}[h_{ABC} + T_2 + T_3]$, then:

$$\mathbb{E}[T_{MRCA}] = \omega_1 a + 3\omega_2 b,$$

where each mixture component corresponds to the expected gene tree height multiplied by its specific probability ω, noting that $\sum_i \omega_i = 1$, $\omega_1 + \omega_2 = P(G_c)$ and $\omega_2 = P(G_{dis_1}) = P(G_{dis_2})$. Now we evaluate all pairwise comparisons of $\mathbb{E}[T_{MRCA}]$ between discordant and concordant topologies, i.e. $R_1 = \frac{\mathbb{E}_{G_c}[T_{MRCA}]}{\mathbb{E}_{G_{dis1}}[T_{MRCA}]}$, $R_2 = \frac{\mathbb{E}_{G_c}[T_{MRCA}]}{\mathbb{E}_{G_{dis2}}[T_{MRCA}]}$, $R_3 = \frac{\mathbb{E}_{G_{dis1}}[T_{MRCA}]}{\mathbb{E}_{G_{dis2}}[T_{MRCA}]}$.

$$\mathbb{E}_{G_c}[T_{MRCA}] = \frac{\omega_1 a + \omega_2 b}{\omega_1 + \omega_2}, \ \mathbb{E}_{G_{dis1}}[T_{MRCA}] = b, \ \mathbb{E}_{G_{dis2}}[T_{MRCA}] = b. \quad (5)$$

In this null case $\mathbb{E}_{G_c}[T_{MRCA}] < \mathbb{E}_{G_{dis1}}[T_{MRCA}]$, since $b > a$, unless the probability of $\omega_1 = P^{(2)}_{0,AB} \to 0$, i.e. for the internal branch length $\Delta h \to 0$ or $\theta_{AB} \to \infty$. The same result follows for the $\mathbb{E}_{G_c}[T_{MRCA}]$ vs. $\mathbb{E}_{G_{dis2}}[T_{MRCA}]$ comparison. Additionally, under MSC the mixture components for discordant topologies G_{dis1} and G_{dis2} are expected to have equal expectations for gene tree heights. These disparities between $\mathbb{E}[T_{MRCA}]$'s for various gene tree topologies serve as foundation for the tree height test (THT) comparison (see below).

For the second scenario (**Fig 1b**), i.e. the multispecies coalescent with introgression model (MSCi) (Yu et al. 2014c), we allow a bidirectional gene flow to occur between non-sister species B and C, with the probabilities of outflow and inflow $\Gamma = (\gamma_1, \gamma_2)$. Specifically, for instance the γ_1 can be interpreted as the probability of a gene copy in species B "slipping" via introgression "bridge" into the population of species C, whereas $1 - \gamma_1$ will correspond to the probability of gene copy in species B staying in population B. Note that under the formulation of the MSCi model here the introgression takes place only at fixed time points, thus it represents a special case of a more general multispecies network coalescent model (Zhu and Degnan 2017). As in MSC we define $\Theta = (\theta_A, \theta_B, \theta_C, \theta_{AB}, \theta_{ABC})$ and $h = (h_{AB}, h_{ABC}, h_i)$ where h_i denotes not a divergence time but rather a time of the introgression event; hence, if gene copy B ends up in

population C the probability that gene copies B and C don't coalesce in population C (and vise versa) is:

$$P^{(2)}_{0,C} = e^{-\frac{2}{\theta_c}(h_{ABC} - h_i)}, \quad (6)$$

$$P^{(2)}_{0,B} = e^{-\frac{2}{\theta_c}(h_{AB} - h_i)}. \quad (7)$$

Following similar logic as for MSC, we can derive probabilities of concordant and discordant topologies:

$$\begin{aligned} P(G_c) = {} & (1-\gamma_1)(1-\gamma_2)(1-\tfrac{2}{3}P^{(2)}_{0,AB}) \\ & + \gamma_1(1-\gamma_2)(\tfrac{1}{3}P^{(2)}_{0,C}) \\ & + \gamma_2(1-\gamma_1)(\tfrac{1}{3}P^{(2)}_{0,B}) \\ & + \gamma_1\gamma_2(\tfrac{1}{3}P^{(2)}_{0,AB}), \quad (8) \end{aligned}$$

$$\begin{aligned} P(G_{dis1}) = {} & (1-\gamma_1)(1-\gamma_2)(\tfrac{1}{3}P^{(2)}_{0,AB}) \\ & + \gamma_1(1-\gamma_2)(1-\tfrac{2}{3}P^{(2)}_{0,C}) \\ & + \gamma_2(1-\gamma_1)(1-\tfrac{2}{3}P^{(2)}_{0,B}) \\ & + \gamma_1\gamma_2(\tfrac{1}{3}P^{(2)}_{0,AB}), \quad (9) \end{aligned}$$

$$\begin{aligned} P(G_{dis2}) = {} & (1-\gamma_1)(1-\gamma_2)(\tfrac{1}{3}P^{(2)}_{0,AB}) \\ & + \gamma_1(1-\gamma_2)(\tfrac{1}{3}P^{(2)}_{0,C}) \\ & + \gamma_2(1-\gamma_1)(\tfrac{1}{3}P^{(2)}_{0,B}) \\ & + \gamma_1\gamma_2(1-\tfrac{2}{3}P^{(2)}_{0,AB}). \quad (10) \end{aligned}$$

In contrast to the MSC, the probability of discordant topologies can differ, specifically:

$$P(G_{dis1}) > P(G_{dis2}),$$

only if

$$\gamma_1(1-\gamma_2)(1-P^{(2)}_{0,C}) + \gamma_2(1-\gamma_1)(1-P^{(2)}_{0,B}) > \gamma_1\gamma_2(1-P^{(2)}_{0,AB}).$$

It is straightforward to show that for the special case of a unidirectional introgression i.e. $\gamma_1 = 0$ (or $\gamma_2 = 0$), the $P(G_{dis1}) > P(G_{dis2})$ will hold unless $P^{(2)}_{0,B} \to 1$ (or $P^{(2)}_{0,C} \to 1$).

Now we define the $\mathbb{E}[T_{MRCA}]$ for the MSCi model (see Appendix for more details) and denote $\mathbb{E}_{\theta_{ABC}}[h_{ABC} + T_2] = a$, $\mathbb{E}_{\theta_{ABC}}[h_{ABC} + T_2 + T_3] = b$, $c = \mathbb{E}_{\theta_{AB}}[h_{AB} + T_2 + T_3]$, $d = \mathbb{E}_{\theta_{AB}}[h_{AB} + T_2]$, where $d < c < a < b$, then:

$$\begin{aligned}\mathbb{E}[T_{MRCA}] = {} & (1 - \gamma_1)(1 - \gamma_2)(\omega_1 a + 3\omega_2 b) \\ & + \gamma_1 (1 - \gamma_2)(\omega_9 a + 3\omega_3 b) \\ & + \gamma_2 (1 - \gamma_1)(\omega_{11} d + 3\omega_4 c + (3\omega_5 + \omega_{14}) a + 3\omega_6 b) \\ & + \gamma_1 \gamma_2 (\omega_1 a + 3\omega_2 b).\end{aligned}$$

In the next step we examine all pairwise comparisons of weighted expectations like in the MSC case. Contrary to the MSC model, however, the R_1, R_2 and R_3 expectation ratios derived from MSCi may exhibit non-trivial dependency on the combination of model parameters (**Fig. 2**, **supplementary Fig. S1**). Based on this observation, we need to determine which of those ratios has the highest power to detect introgression, i.e., the ratio that on average deviates from unity the most. To that end, we performed 10^5 Monte Carlo simulations to evaluate to what extent each ratio deviates from one by calculating difference between expectation ratio and one, i.e. $R - 1$. For each iteration, to simulate a value of the expectation ratio we sampled a set of model parameters from uniform distributions $U(0, 1)$ (**Fig. 3**). The simulation results indicate that R_1 has the highest deviation from one (mean = 0.184 and median = 0.091). This suggests that comparisons of gene tree height expectations derived from concordant topologies ($\mathbb{E}_{G_c}[T_{MRCA}]$) and discordant topologies 1 ($\mathbb{E}_{G_{dis1}}[T_{MRCA}]$) will likely exhibit higher statistical power (i.e. the probability of correctly rejecting the null MSC model if MSCi is true) compared to other expectation ratios. Additionally, we estimated how many times each expectation ratio is greater or smaller than one. Analyzing the simulation results we found that $R_1 > 1$ in $\sim 90.9\%$, $R_2 > 1$ in $\sim 49.9\%$ and $R_3 > 1$ in $\sim 9\%$.

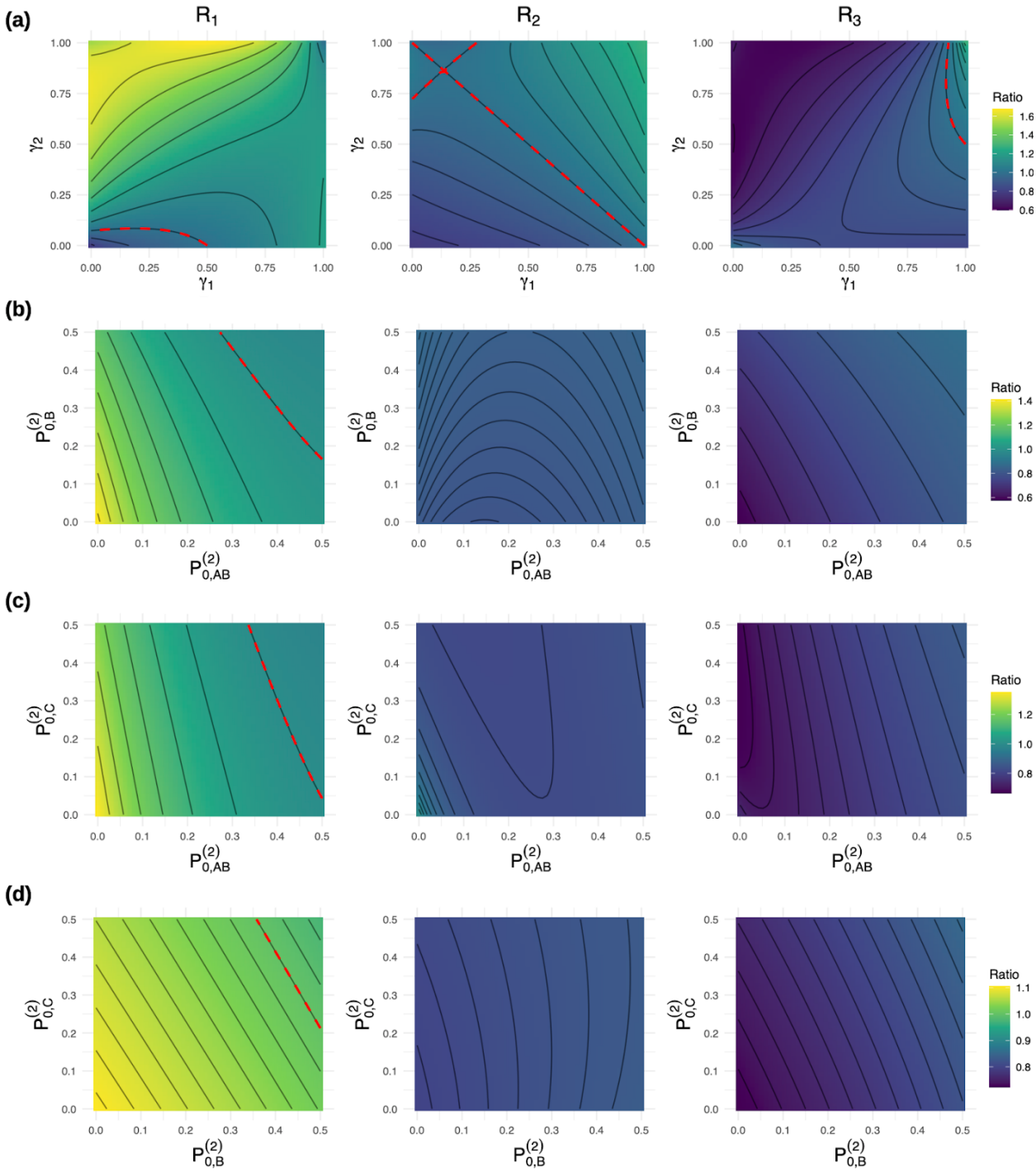

Fig. 2 Contour plots of the expectation surface under MSCi model : a) - d) The changes of expectation ratio values in respect to the varying parameters of the MSCi model. The R_1 trough R_3 represent expectation ratios, i.e. $R_1 = \frac{\mathbb{E}_{G_c}[T_{MRCA}]}{\mathbb{E}_{G_{dis1}}[T_{MRCA}]}$, $R_2 = \frac{\mathbb{E}_{G_c}[T_{MRCA}]}{\mathbb{E}_{G_{dis2}}[T_{MRCA}]}$, $R_3 = \frac{\mathbb{E}_{G_{dis1}}[T_{MRCA}]}{\mathbb{E}_{G_{dis2}}[T_{MRCA}]}$. The red dashed line marks the region where expectation ratios attain unity. $P^{(2)}_{0,AB}$, $P^{(2)}_{0,B}$ and $P^{(2)}_{0,C}$ denote the probabilities of two lineages not coalescing in the populations AB, B or C, respectively. The γ_1 and γ_2 parameters represent introgression probabilities. Only two parameters were being

varied at a time, while the rest were fixed at $\gamma_1 = 0.1$, $\gamma_2 = 0.1$, $P^{(2)}{}_{0,A} = P^{(2)}{}_{0,B} = P^{(2)}{}_{0,C} = 0.3$, $a = 0.3$, $b = 0.4$, $c = 0.2$, $d = 0.1$.

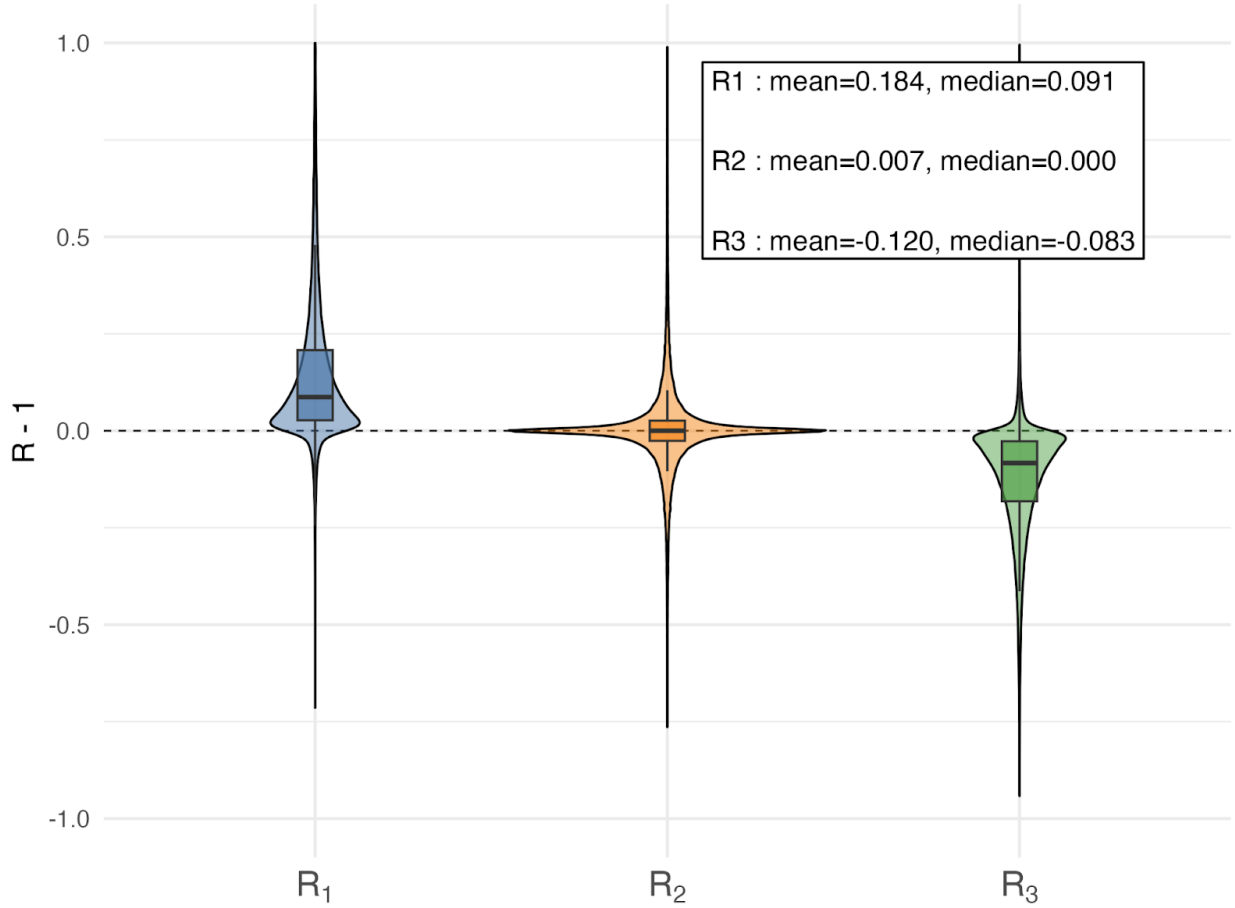

Fig. 3 Distribution of simulated expectation ratios under MSCi : Violin plots represent simulated distributions of the $R - 1$ values for each of the expectation ratios, i.e. $R_1 = \frac{\mathbb{E}_{G_c}[T_{MRCA}]}{\mathbb{E}_{G_{dis1}}[T_{MRCA}]}$, $R_2 = \frac{\mathbb{E}_{G_c}[T_{MRCA}]}{\mathbb{E}_{G_{dis2}}[T_{MRCA}]}$, $R_3 = \frac{\mathbb{E}_{G_{dis1}}[T_{MRCA}]}{\mathbb{E}_{G_{dis2}}[T_{MRCA}]}$. The box plot within each violin shows median as well as lower and upper quantiles. The dashed line marks the $R - 1$ values of zero.

Finally, we consider the multispecies coalescent with introgression scenario (MSCig) where gene flow occurs exclusively between the contemporary lineage A and an extinct/unsampled ("ghost") lineage X (**Fig. 1c**). Furthermore, we assume that there is no introgression between neither C and A nor C and B. Since the gene copy from X is not sampled, only outflow introgression from A to X is parametrized by probability γ. For this model we define $\Theta = (\theta_A, \theta_B, \theta_C, \theta_G, \theta_{AB}, \theta_{ABC}, \theta_{ABCX})$ and $H = (h_{AB}, h_{ABC}, h_{ABCX})$. Given the parametrization of the MSCig we can derive frequencies of concordant and discordant gene tree topologies as follows:

$$P(G_c) = (1 - \gamma)(1 - \frac{2}{3}P^{(2)}{}_{0,AB}) + \gamma(\frac{1}{3}P^{(2)}{}_{0,ABC}),$$
$$P(G_{dis1}) = (1 - \gamma)(\frac{1}{3}P^{(2)}{}_{0,AB}) + \gamma(1 - \frac{2}{3}P^{(2)}{}_{0,ABC}),$$
$$P(G_{dis2}) = (1 - \gamma)(\frac{1}{3}P^{(2)}{}_{0,AB}) + \gamma(\frac{1}{3}P^{(2)}{}_{0,ABC}).$$

In the case of the MSCig model the difference of discordant topology probabilities will not depend on γ (unless $\gamma = 0$, which will reduce MSCig to MSC null model where $P(G_{dis1}) = P(G_{dis2})$) or $P_{0,AB}$, i.e.

$$P(G_{dis1}) > P(G_{dis2}),$$

only if

$$P^{(2)}{}_{0,ABC} < 1.$$

In other words, the frequency of discordant gene tree topologies G_{dis1} will be always greater than frequency of G_{dis1} unless $\theta_{ABC} \to \infty$ or $\Delta h = h_{ABCX} - h_{ABC} \to 0$. Next we formulate the $\mathbb{E}[T_{MRCA}]$ for the MSCig model (see Appendix for more details) with $\mathbb{E}_{\theta_{ABC}}[h_{ABC} + T_2] = a$, $\mathbb{E}_{\theta_{ABC}}[h_{ABC} + T_2 + T_3] = b$, $\mathbb{E}_{\theta_{ABCX}}[h_{ABCX} + T_2] = c$, $\mathbb{E}_{\theta_{ABCX}}[h_{ABCX} + T_2 + T_3] = d$, where $a < b < c < d$, then:

$$\mathbb{E}[T_{MRCA}] = (1 - \gamma)(\omega_1 a + 3\omega_2 b + (\omega_3 + 3\omega_4)c + 3\omega_5 d) + \gamma(\omega_4 c + 3\omega_6 d).$$

As in the case of the MSCi model the expectation ratios have complex relationships with the combinations of model parameters (**Fig. 4**). Again, based on the Monte Carlo simulation for the MSCig model, we determined that the R_2 ratio only marginally outperformed R_1 ratio using mean and median criteria of $R - 1$ distributions (**Fig. 5**). As for the MSCi model, here we calculated how many times the expectation ratios are greater or smaller than one in simulations. This analysis yielded $R_1 > 1$ in $\sim 14.9\%$, $R_2 > 1$ in $\sim 0.7\%$ and $R_3 > 1$ in $\sim 29.2\%$. Nevertheless, because the same gene tree height expectation comparisons must be used consistently across

all three models (MSC, MSCi, and MSCig), we selected the R_1 ratio as the basis. R_1 shows markedly larger deviations under MSCi than R_2, which in turn performs worse than R_3. Moreover, because the values of R_1 tend to exceed one under MSCi but fall below one under MSCig (Fisher's exact test, odds ratio = 56.76, 95% CI: 55.2-58.3, $P \sim 0$) in simulations, this property can be used to distinguish the two models: $\mathbb{E}_{G_c}[T_{MRCA}] > \mathbb{E}_{G_{dis2}}[T_{MRCA}]$ for MSCi, whereas $\mathbb{E}_{G_c}[T_{MRCA}] < \mathbb{E}_{G_{dis2}}[T_{MRCA}]$ for MSCig with a success probability of ~78.7%.

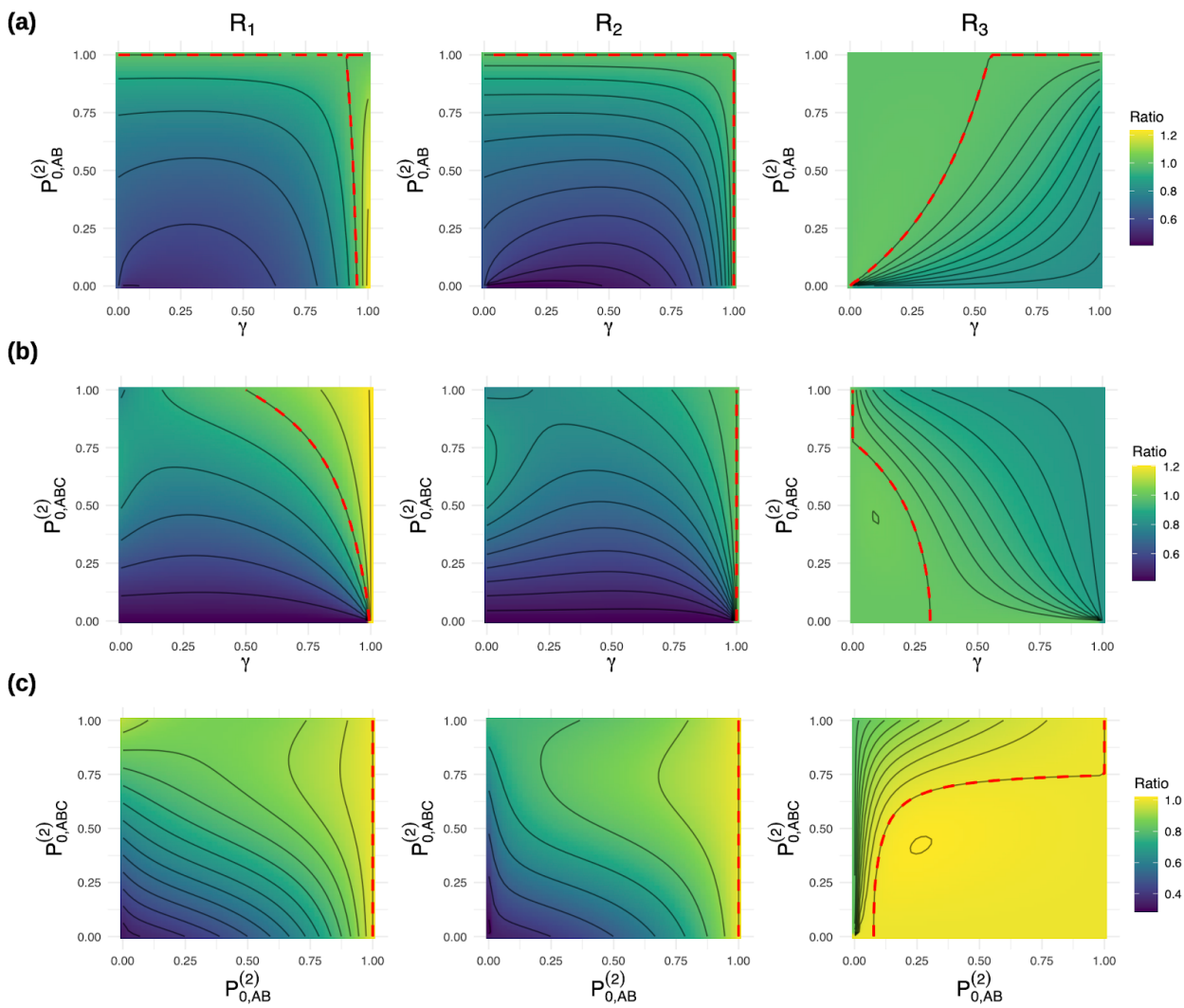

Fig. 4 Contour plots of the expectation surface under MSCig model : a) - c) The changes of expectation ratio values in respect to the varying parameters of the MSCig model. The R_1 trough R_3 represent expectation ratios, i.e. $R_1 = \frac{\mathbb{E}_{G_c}[T_{MRCA}]}{\mathbb{E}_{G_{dis1}}[T_{MRCA}]}$, $R_2 = \frac{\mathbb{E}_{G_c}[T_{MRCA}]}{\mathbb{E}_{G_{dis2}}[T_{MRCA}]}$, $R_3 = \frac{\mathbb{E}_{G_{dis1}}[T_{MRCA}]}{\mathbb{E}_{G_{dis2}}[T_{MRCA}]}$. The red dashed line marks the region where expectation ratios

attain unity. $P^{(2)}_{0,AB}$ and $P^{(2)}_{0,ABC}$ denote the probabilities of two lineages not coalescing in the populations AB or ABC, respectively. The γ parameter represents introgression probability. Only two parameters were being varied at a time, while the rest were fixed at $\gamma = 0.1$, $P^{(2)}_{0,AB} = 0.3$, $P^{(2)}_{0,ABC} = 0.3$, $a = 0.1$, $b = 0.2$, $c = 0.3$, $d = 0.4$.

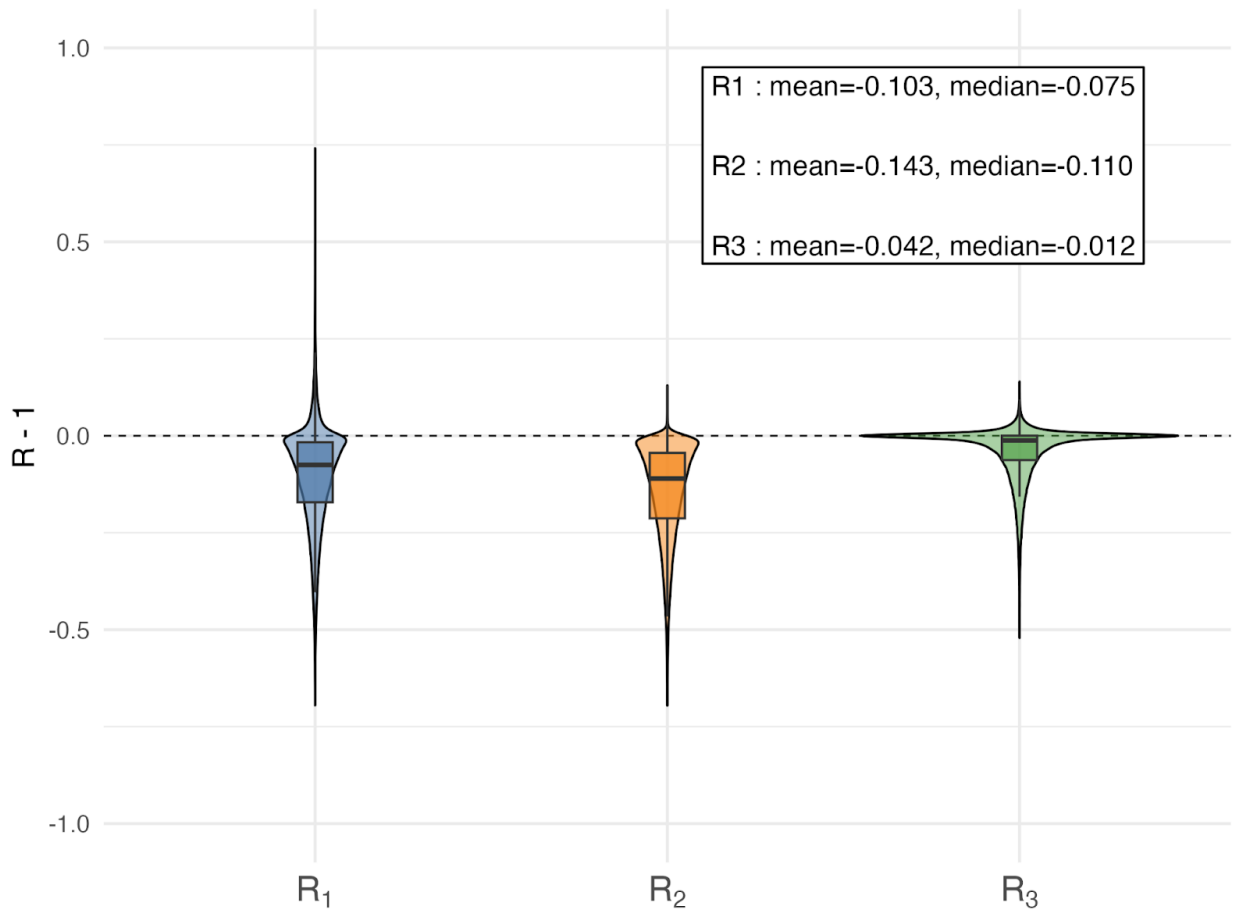

Fig. 5 Distributions of simulated expectation ratios under MSCig violin introgression: Violin plots represent simulated distributions of the $R - 1$ values for each of the expectation ratios, i.e. $R_1 = \frac{\mathbb{E}_{G_c}[T_{MRCA}]}{\mathbb{E}_{G_{dis1}}[T_{MRCA}]}$, $R_2 = \frac{\mathbb{E}_{G_c}[T_{MRCA}]}{\mathbb{E}_{G_{dis2}}[T_{MRCA}]}$, $R_3 = \frac{\mathbb{E}_{G_{dis1}}[T_{MRCA}]}{\mathbb{E}_{G_{dis2}}[T_{MRCA}]}$. The box plot within each violin shows median as well as lower and upper quantiles. The dashed line marks the $R - 1$ values of zero.

Finally, to obtain approximations of tree height (T_{MRCA}) for each gene tree triplet we used summary statistic $H(T)$, which represents the average of tree distances between each tip and the root node, i.e.

$$T_{MRCA} \approx H(T) = \frac{b_1 + 2b_2 + b_3 + b_4}{3}$$

where b_1, b_2, b_3 and b_4 denote branch lengths. The b_2, b_3 and b_4 indicate two sister species and their ancestral branch, respectively, whereas b_1 is the remaining branch that connects to the root node, for example $((B: b_2, C: b_3): b_4, A: b_1)$. Our statistic $H(T)$ is related to Sackin index (King and Rosenberg 2021), which is a tree balance statistic representing the sum of all paths from tip to root node on a tree. Thus, $H(T)$ can be viewed as a normalized Sackin index. By measuring gene tree height as the average distance from all three tips to the root node, (i.e. weighting them equally) we attempt to minimize the bias effect of rate variation between lineages (Frankel and Ané 2023).

The GhostParser Pipeline

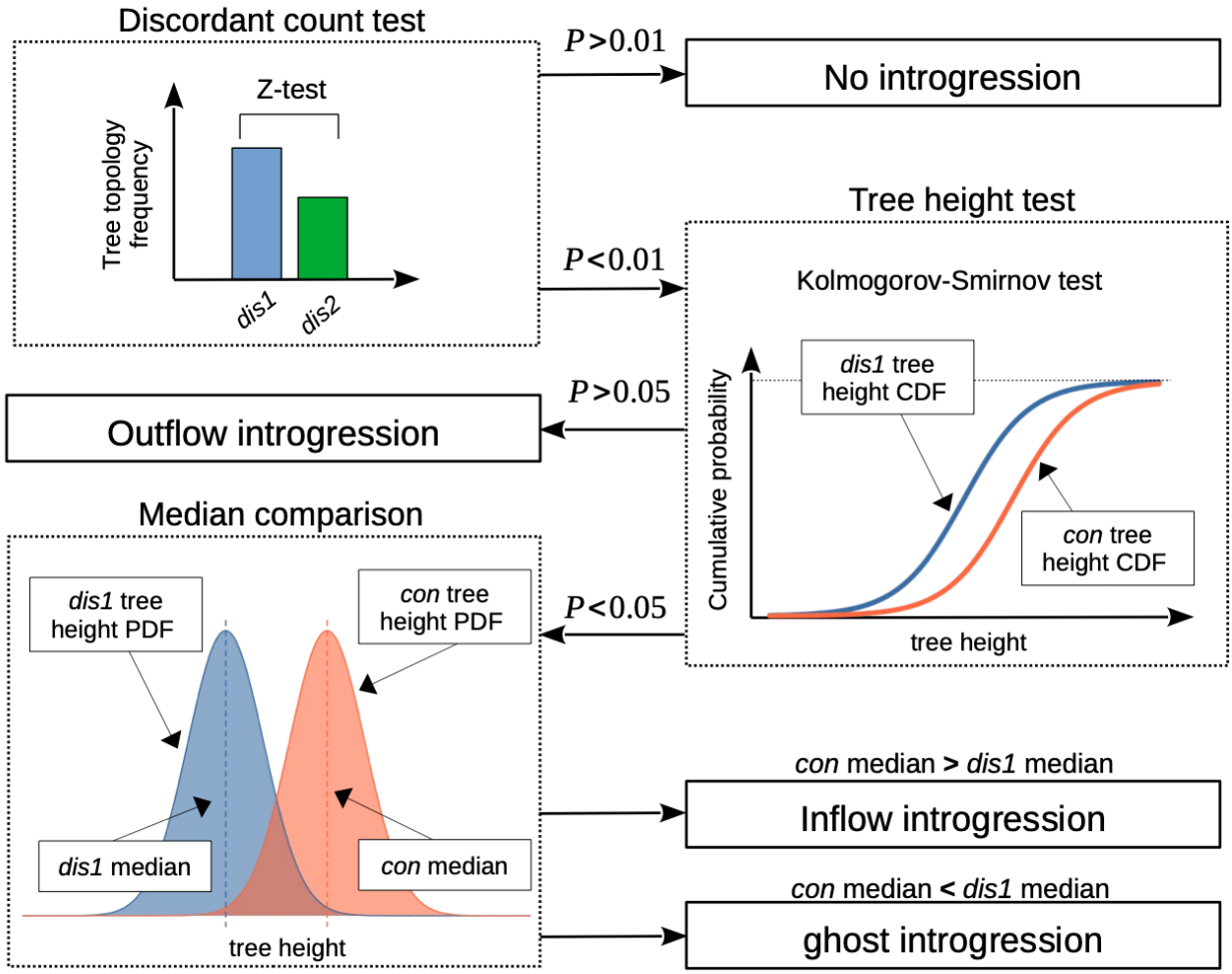

Fig. 6 GhostParser pipeline: The GhostParser pipeline follows a sequential hypothesis testing procedure. Key statistical steps are shown in dashed outline boxes, while specific outcomes are shown in solid boxes. PDF = probability density function, CDF = cumulative distribution function, dis1 = discordant topology 1, i.e. ((B,C),A), dis2 = discordant topology 2, i.e. ((A,C),B), con = concordant topology, i.e. ((A,B),C).

In its core the GhostParser pipeline implements a sequential hypotheses testing procedure (**Fig. 6**) for a rooted species triplet. First, GhostParser compares the frequencies of discordant topologies $P(G_{dis1}) \vee P(G_{dis2})$ using the two proportion Z-test with significance level $\alpha = 0.01$ (such stringent cutoff is used to reduce the occurrence of false positives), which is a variation of Discordant Count Test (DCT; **Fig. 6**; Suvorov et al. 2022A,B) that is based on χ^2 test. If this comparison is statistically significantly different then, GhostParser proceeds to comparison of the difference between $H(T)$ distributions generated from the G_c and G_{dis1} gene trees (effectively we

are comparing $\mathbb{E}_{G_c}[T_{MRCA}]$ and $\mathbb{E}_{G_{dis1}}[T_{MRCA}]$), otherwise GhostParser is unable to reject the null hypothesis (i.e., the MSC model), and therefore shows no evidence for introgression. To root each triplet-specific gene tree and calculate $H(T)$ GhostParser uses ete3 v3.1.3 (Huerta-Cepas et al. 2016) and newick_utils v1.6 (Junier 2024). Then, the resulting $H(T)$ distributions obtained from a set of G_c and G_{dis1} gene trees are compared using Tree Height Test (THT) based on the two sample Kolmogrov-Smirnov test with $\alpha = 0.05$, implemented in R v4.4.2 (R Core Team 2021). If this test does not reject the null hypothesis – i.e. distributions of tree heights from of G_c and G_{dis1} gene tree sets are similar – GhostParser will suggest sampled introgression has occurred without any evidence of inflow introgression. Further, when THT generates significant result we compare the medians of $H(T)$ distributions to differentiate between sampled and ghost introgression scenarios. We note that although theoretical expectations were expressed as means, in practice we compare medians of $H(T)$ distributions, which provide a more robust basis for distinguishing between sampled and ghost introgression. Specifically, if $\mathbb{E}_{G_c}[T_{MRCA}] > \mathbb{E}_{G_{dis1}}[T_{MRCA}]$, then GhostParser infers sampled inflow introgression (can be with or without outflow), but if $\mathbb{E}_{G_c}[T_{MRCA}] < \mathbb{E}_{G_{dis1}}[T_{MRCA}]$ the GhostParser would predict ghost introgression.

The GhostParser pipeline represents a python script which uses a combination of python and R languages. In order to launch GhostParser analysis the user provides the following: (i) an input file with gene trees including branch lengths, one per line in newick format, (ii) a text file that contains a outgroup taxa used to root the triplet, and (iii) the rooted species tree topology in newick format. The user may also provide an optional file with the specific triplets of interest for testing. If this optional file is provided, GhostParser will only analyze each user-specified triplet. Otherwise, it will, by default, analyze every possible triplet from the species tree (excluding the

433 triplets that contain an outgroup taxon). GhostParser will classify each of the three taxa in the
434 triplet as the A, B, or C taxon. For any species triplet, the A and B taxa are always defined as
435 sister in concordant gene tree, whereas the B taxon is sister to C in the most common discordant
436 topology.

437 GhostFinder is an optional follow-up analysis to GhostParser. It uses the output from
438 GhostParser—which identifies recipients of ghost introgression—to search for the potential
439 "ghost" lineage in the species tree. It identifies, from the GhostParser output file, the triplets
440 where evidence of unsampled introgression has been found. It takes each pairing of A and B,
441 where the A taxon is the hypothesized to be a putative recipient of ghost introgression, and the
442 outgroup in G_{dis1}. It then tests all possible C taxa from the species tree to determine if any C taxa
443 will change the assignments of the sister taxa in the triplet. In instances where the putative ghost
444 recipient is reassigned as the B taxon, GhostFinder uses GhostParser to determine which of
445 these C taxa show evidence of inflow introgression with the putative ghost, and flag these
446 introgression donors as putative ghost lineages.

447

448 **Simulations**

449 Here, we generally followed the simulation approach used by Pang and Zhang (2024) to assess
450 the accuracy of GhostParser, and compared its performance against BPP, which more accurately
451 distinguishes between ghost and sampled introgression than all other methodologies designed to
452 detect both of those introgression scenarios. Since inter-lineage rate variation can generate false
453 positive results when using gene tree summary statistics to detect introgression, we incorporated
454 both inter-lineage and inter-locus rate variation into our simulations to enhance biological
455 realism, following the strategy of Frankel and Ané (2023).

456 *Simulating gene trees under differing multispecies coalescent models*

457 To maintain consistency in our simulated dataset and the dataset used to test the accuracy of

BPP, we generated our simulated dataset using a modified perl script (`msplus.pl`) from Pang and Zhang's (2024) work that they used to test the utility of BPP for introgression detection. As originally written, the script uses the *ms* simulator (Hudson 2002) to simulate 480 sets of 1,000 gene trees along a triplet species network topology. The gene tree sets are generated under ghost, inflow and outflow introgression with specific user-provided introgression probabilities. Specifically, this pipeline generates gene tree sets under eight different combinations of species tree branch lengths, with 20 independent replicates per combination of introgression model and branch lengths. We modified this script to include an additional null model, i.e. MSC, as described below. Here we generated total of 620 sets of 1,000 gene trees each for each of the coalescent models, i.e. MSC, MSCi (outflow), MSCi (inflow) and MSCig.

Each set of gene trees was simulated from a species tree topology of $(X,((A,B),C))$, where X is an unsampled "ghost" lineage in *ms*. The event times, such as species divergencies and introgressions are specified directly in coalescent units, where 1 unit corresponds to $4N_e$ generations for a diploid population. We therefore set all event times in these scaled units without specifying N_e explicitly. The distance between MRCA of $ABCX$ and MRCA of ABC was always set to 5 coalescent units, while the internal branch length of AB, the distance between the MRCA of AB and an introgression event involving either A or B, and the distance between the introgression event and the tree tips are all set at either 0.5 or 5 coalescent units. This results in a total of eight possible branch-length combinations. To simulate aforementioned gene tree sets we used MSC ($\gamma_1 = \gamma_2 = \gamma = 0$), MSCi (outflow; $\gamma_1 \in [0,1]$, $\gamma_2 = \gamma = 0$), MSCi (inflow; $\gamma_2 \in [0,1]$, $\gamma_1 = \gamma = 0$) and MSCig ($\gamma \in [0,1]$, $\gamma_1 = \gamma_2 = 0$) models with corresponding introgression probabilities Γ. Further, for each possible combination of coalescent model and branch-lengths, 20 independent replicates were generated, for a total of 640 sets of 1000 gene trees each. We produced the simulated gene trees under high ($\Gamma = 0.3$, $\Gamma = 0.5$), moderate ($\Gamma = 0.1$) and low ($\Gamma = 0.05$, $\Gamma = 0.01$) values of introgression probabilities, where

$\Gamma = (\gamma_1, \gamma_2, \gamma)$. In summary, this amounted to a total of 3,200 sets of 1,000 gene trees each under every possible combination of introgression probability, timing, and coalescent model including 20 independent replicates.

Incorporating rate variation between lineages

To test how GhostParser performs in the presence of rate variation, which can result in false positives of both sampled and ghost introgression, we implemented an approach used by Frankel and Ané (2023) to introduce rate variation into the terminal branches of simulated gene trees. Specifically, for every set of 1,000 gene trees, we first pruned the ghost taxon X, then we assigned a rate multiplier for each terminal branch in the species tree $((A, B), C)$. These rate multipliers were drawn independently from a log-normal distribution ($\mu = 1.0$, $\sigma = 0.7$), with a maximum allowed value of four. We then multiplied the branch lengths (expressed in coalescent units) in each of the 1,000 gene trees by the branch rate multiplier.

Generating multiple sequence alignments

In generating multiple sequence alignments (MSAs) for each set of 1,000 uniformly rate-modified gene trees, we additionally incorporated intergeneric rate variation, which is observed in empirical multi-locus datasets (Yang 1996; Phillips et al. 2004). We generated each MSA with AliSim (Ly-Trong et al. 2022), implemented in IQ-TREE2 v2.3.6 (Minh et al. 2020). To convert branch lengths from our rate-modified coalescent units to substitutions per site as well as to include intergenic rate variation in each 1,000 gene dataset, we sampled the rate-scaling factor for each locus independently from a Gaussian distribution ($\mu = 0.036$, $\sigma = 0.003$). The scaling factor $\theta = 4N_e\mu$ thus, assuming a constant N_e, drawing the scaling factor independently from a distribution imbues variation in per-site mutation rate μ_g. To maintain consistency with Pang and Zhang's (2024) simulations, we used the HKY nucleotide substitution model, which assumes unequal transition and transversion rates, and unequal base frequencies (Hasegawa et al. 1985). By default, AliSim assigns transition and transversion rate parameters, as well as base

frequencies for the HKY model by drawing corresponding parameters form empirical distributions estimated from a large dataset consisting of different loci (e.g. codon positions, rR 203, Column 3NA, rTNA, introns, intergenic spacers, and UCEs) and genomes (nuclear, mitochondria, virus, and plastid) sampled across the Tree of Life (Naser-Khdour et al. 2025). The alpha parameter for the gamma distribution, which controls rate variation among sites, was drawn from a log-normal distribution, scaled by the the proportion of invariant sites (I) to reflect the relationship between these two parameters ($\mu = -0.2 + (\frac{I}{2.5})$, $\sigma = 0.5$) with minimum and maximum constraints of 0.2 and 5.0 to avoid biologically unrealistic values for each gene. To incorporate realistic among-site rate heterogeneity, we modeled the proportion of invariant sites (I) as a random variable drawn from a Beta distribution ($\alpha = 5$, $\beta = 10$) which was then scaled by 0.5. These specific parameters produce a right-skewed distribution favoring lower to intermediate proportions of invariant sites, reflecting patterns observed in many empirical datasets where most sites evolve at non-zero rates but some remain highly conserved (Yang 1994; Yang 1996). The additional 0.5 scaling limits invariant sites to at most half the MSA length, maintaining sufficient phylogenetic signal while still allowing considerable conservation. To incorporate insertion and deletion events into our simulations, we drew insertion and deletion rates separately from a Gaussian distribution ($\mu = 0.005$, $\sigma = 0.00156$), with a hard lower bound of zero to prevent the proportions from being assigned negative values. Each simulated MSA contained 1000 sites.

Estimating Gene Trees

As errors in inferred MSA can affect gene tree inference (Ogden and Rosenberg 2006; Wong et al. 2008), we realigned every simulated loci with MAFFT v7.525 (Katoh and Standley 2013) with the option *--linsi* to ensure better MSA inferential accuracy. We then estimated maximum likelihood gene tree topologies from the simulated MSAs using IQ-TREE2 v2.3.6 (Minh et al. 2020) under the best fitting substitution model. Finally, we tested GhostParser's performance on

533 the dataset.

534 *Additional testing of potentially problematic demographic scenarios*

535 It has been noted that DCT and BLT based methods could, theoretically, be influenced by
536 ancestral population structure (Suvorov et al. 2022A). Particularly in a scenario where the true
537 species tree is $((A, B), C)$, but B and C share a more recent MRCA, and A introgressed with
538 common ancestor of B and C with a continued gene flow with B following the split of B and C. The
539 current understanding is that such a phenomenon may be unlikely (Suvorov et al. 2022A),
540 nonetheless in addition to our *ms* simulated dataset, we generated 500 such scenarios with
541 msprime v1.3.3 (Baumdicker et al. 2022). For each scenario, the MRCA of ABC in the species
542 tree was selected from a uniform distribution of between 1 and 50 million generations before
543 present. The A lineage and the ancestral branch BC each generated gene flow into the other
544 population with the introgression probability drawn from a random uniform distribution between
545 10^{-6} and 0.5 until a random time between the MRCA of ABC and 90% of the MRCA of ABC, when
546 B and C diverged. A and B continued to hybridize, the introgression probability from each
547 population again chosen from a uniform distribution between 10^{-6} and 0.5 until a random time
548 between the MRCA of BC and 90% of the MRCA of BC, when gene flow stopped. The N_e of ABC,
549 the MRCA of C and B, and the MRCA of A, B and C were selected from a uniform distribution
550 *U*(50,000, 5,000,000). The outgroup taxa used to root the triplet was always constrained to
551 diverge with ABC 10 million generations prior to the MRCA of ABC, and had an N_e of 500,000.
552 Under each scenario we simulated 1000 gene trees with branch lengths measured in coalescent
553 units. As we only consider the impact of demographic history here, we used the simulated gene
554 trees directly as input for GhostParser testing the hypothesis that A was the recipient of ghost
555 introgression or that B and C introgressed.

556 ***Comparing GhostParser and BPP***

557 We examined the performance of GhostParser on each simulated dataset generated by ms. In

contrast to GhostParser, model selection in BPP is computationally intensive—6 CPU-hours per dataset to compare ghost, inflow, and outflow models (Pang & Zhang, 2024). Given this computational cost and our inclusion of an additional no-introgression model, we evaluated BPP only on a subset of simulated datasets. To estimate the performance of BPP in a broad range of scenarios we considered only five of the replicates for each unique combination of timing, introgression probability and coalescent model, instead of the 20 total replicates used to test GhostParser. Additionally, we did not evaluate the performance of BPP in the potentially problematic demographic scenario nor in the scenario of lowest introgression probability (i.e. $\Gamma = 0.01$). We built the multispecies coalescent with introgression (MSci) scenario to test each of the coalescent models (i.e. MSC, MSCi inflow, MSCi outflow and MSCig) using the "msci-create" function from BPP (see **supplementary table 1** for full commands). We used the same demographic parameters as in Pang and Zhang (2024). Specifically, we used Gaussian quadrature combined with thermodynamic integration to calculate the marginal likelihoods of each scenario. We ran a total of 1.05×10^6 iterations, using the first 50,000 MCMC iterations as burn-in, and then sampling every other iteration. We then estimated the optimal parameters of the MSci model using the A00 analysis built into BPP (Yang 2015; Pang and Zhang 2024). Each BPP analysis was executed twice to ensure model convergence.

We compared the performance of BPP and GhostParser under each tested level of Γ (with the exception of level of $\Gamma = 0.01$ upon which BPP was not tested). For each tested level of Γ, we calculated the specificity (true negatives/(true negatives + false positives)) and sensitivity (true positives/(true positives + false negatives)) diagnostic metrics of both BPP and GhostParser for our four tested introgression models. We also calculated the overall accuracy for both BPP and GhostParser for each compared level of Γ both when considering inflow and outflow as separate categories, and when considering them as one category of "sampled introgression."

583 Since previous study (Pang and Zhang 2024) indicates that BPP exhibits markedly better
584 performance than other methods designed to differentiate between ghost and sampled
585 introgression (e.g. HyDe (Blischak et al. 2018), SNaQ (Solís-Lemus et al. 2017) and PhyloNet (Li
586 et al. 2022)), we did not consider any other software comparisons.

587 ***Empirical datasets***

588 To further benchmark GhostParser against BPP, we ran GhostParser on two empirical
589 phylogenomic datasets – two plant genera *Jaltomata* and *Thuja* – which were used by BPP in
590 the original study. In each empirical dataset we used previously identified introgression events as
591 guiding hypotheses for GhostParser. Additionally, for each identified reticulation event in each
592 dataset, we calculated the proportion of triplets that support the proposed introgression
593 hypothesis, which can provide a measure of confidence in the inferred introgression event
594 (Suvorov et al., 2022A).

595

596 *Jaltomata*

597 *Jaltomata* is a plant genus of approximately 60 species in the family Solanaceae, which contains
598 subgroups distinguished by mature fruit colors, and has experienced recent radiations (Miller et
599 al. 2011). Using BPP, Pang and Zhang (2024) identified three nodes in the phylogeny of
600 *Jaltomata* influenced by introgression, in a transcriptomic dataset containing 14 species from the
601 genus (Wu et al. 2018). In comparison, node one was incorrectly identified as a recipient of ghost
602 introgression, by HyDe and SNaQ (Solís-Lemus and Ané 2016; Solís-Lemus et al. 2017),
603 whereas BPP correctly identified sampled introgression. The second and third nodes were
604 identified as sampled introgression by BPP, SNaQ and HyDe. The gene trees provided in Pang
605 and Zhang (2024) were used as input for GhostParser to test for introgression in each of the
606 three previously identified nodes.

607

608 *Thuja*

609 Compared to many taxa in the Tree of Life, the patterns of ghost introgression have been
610 extensively categorized in the coniferous plant genus *Thuja* (Li et al., 2022; Pang and Zhang
611 2024). Li et al., (2022) generated a transcriptomic dataset of 2,969 single-copy genes, for four
612 species of *Thuja*, namely *T. standishii*, *T. sutchuenensis*, *T. plicata* and *T. dolobrata*. Of these
613 four species, *T. dolobrata* is the outgroup, while *T. sutchuensis* and *T. standishi* form sister
614 relationships (Li et al. 2022). Li et al., (2022) identified *T. sutchuenensis* as the recipient of ghost
615 introgression, while HyDe identified introgression between *T. standishi* and *T. plicata* (Pang and
616 Zhang 2024). Pang and Zhang (2024), used BPP to tease apart the competing hypotheses that
617 *T. standishi* and *T. plicata* experienced gene flow, whereas *T. sutchuenensis* was found to be the
618 recipient of ghost introgression. As with the *Jaltomata* dataset, the *Thuja* gene trees provided by
619 Pang and Zhang (2024) were used as the input for GhostParser.
620

621 ***Additional empirical testing of GhostParser***

622 To further demonstrate the utility of GhostParser in empirical systems we tested GhostParser in
623 two clades which are now common examples of widespread introgression. First, identification of
624 introgression across the butterfly genus *Heliconius* was one of the first discoveries to support the
625 hypothesis that introgression played a key role in the radiation of insects (Edelman et al. 2019).
626 Second, the fly genus *Drosophila* exhibits abundant instances of introgression despite evidence
627 for reproductive isolation (Suvorov, et al. 2022A). However, both studies relied on introgression
628 estimation methods that are incapable of identifying ghost introgression and are prone to
629 producing false positive results in the presence of inter-lineage rate variation (Frankel and Ané
630 2023). Here, we use GhostParser to revisit the hypotheses of introgression identified in these
631 systems.

632 *Heliconius*

633 Here, we revisit the hypothesis of sampled introgression in the melpomene clade of *Heliconius*
634 butterflies, using trees generated from a whole genome alignment of *Heliconius* (Edelman et al.

635 2019). We reconsider two introgression events with GhostParser using the original set of gene
636 trees as input, and using triplets from two hypothesized introgression events as guides for
637 hypothesis testing in this classical system, with the tree topology previously estimated by
638 Edelman et al., (2019) as GhostParser input.

639 *Drosophila*

640 The identification of introgression in the fly genus *Drosophila* is among the most promising
641 systems for exploring the functional impacts of introgression, as the genomes of the model
642 species *D. melanogaster* and *D. simulans* are amongst the most well studied in the entire Tree of
643 Life (Suvorov, et al. 2022A). Here, we considered the *Drosophila* gene tree dataset, generated
644 by Suvorov et al. (2022A). The original analysis of this dataset identified numerous putative
645 instances of introgression. In particular, clades three, seven and nine contained two, five and
646 three instances of highly supported inter-specific gene flow respectively. We used this dataset to
647 revisit each of these putative introgression events with GhostParser, and tested an additional six
648 species triplets where no introgression was detected to test for putative false positives. In
649 detected instances of ghost introgression, we employed GhostFinder to search the *Drosophila*
650 tree for possible "ghost" lineages across the entire sampled *Drosophila* dataset, using the
651 species tree estimated by Suvorov et al., (2022A) as input.

652

653 Results

654 ***Comparison of GhostParser and BPP in simulated datasets***

655 The model accuracy of GhostParser was greater than that of BPP both when inflow and outflow
656 introgression were considered to be two separate categories, and when they were combined into
657 one category of sampled introgression, regardless of the introgression probability tested (**Table**
658 **1; Fig. 7**). Both BPP and GhostParser maintained similar accuracy under $\Gamma = 0.50$
659 (GhostParser = 0.91, BPP = 0.71 with inflow and outflow introgression combined) and $\Gamma = 0.30$

(GhostParser = 0.92, BPP = 0.69 with inflow and outflow introgression binned together; **Table 1**). Accuracy for both diminished at $\Gamma = 0.1$ (GhostParser = 0.80, BPP = 0.61 with inflow and outflow introgression binned together) and $\Gamma = 0.05$ (GhostParser = 0.60, BPP = 0.53 with inflow and outflow introgression combined; Table 1). GhostParser performed at random (accuracy = 0.24) under $\Gamma = 0.01$ (BPP was not tested under this introgression probability due to computational constraints; **Table 1; Fig. 7**). GhostParser was more sensitive to ghost introgression under $\Gamma = 0.50$ and $\Gamma = 0.30$, while BPP was more sensitive under the lower strength introgression scenarios (**Table 1**). The specificity of ghost introgression was high (0.88) in both BPP and GhostParser (**Table 1**) under all introgression strengths tested, with GhostParser marginally (difference < 0.10) outperforming BPP in the specificity of ghost introgression, excepting $\Gamma = 0.50$ where both were tied at 0.91 (**Table 1**). BPP was more sensitive to both inflow and outflow introgression than GhostParser (Table 1). GhostParser was much more specific (>0.80) in its detection of inflow introgression than BPP (<0.60). BPP showed higher sensitivity to outflow introgression than GhostParser (**Table 1**). Both were highly specific in their detection of outflow introgression (0.95) with BPP only outperforming GhostParser by a few points. BPP showed low (<0.15) sensitivity to the detection of no introgression, while GhostParser exhibited very high (>0.97) sensitivity to this model (**Table 1**). BPP was highly specific (>0.99) in its detection of no introgression at $\Gamma = 0.50$ and $\Gamma = 0.30$. The specificity of GhostParser under MSC dropped to 0.84 at $\Gamma = 0.1$, to 0.55 at $\Gamma = 0.05$ and to 0.06 at $\Gamma = 0.01$ (Table 1). BPP showed the inverse relationship with the specificity of the detection of the null model, climbing from 0.76 at $\Gamma = 0.50$ to 1.00 at $\Gamma = 0.10$ (**Table 1**).

Additional testing of GhostParser in simulated datasets

In the 500 tested replicates of the continuous gene flow scenario (simulated with msprime to test if population structures could produce false positives in GhostParser. GhostParser found no

evidence for introgression in 96.6% of the simulated triplets and classified 2.0% and 1.4% of the simulated triplets as sampled and ghost introgression respectively.

687

Table 1: Comparison of GhostParser and BPP performance

	MSCig sensitivity	MSCig specificity	MSCi (inflow) sensitivity	MSCi (inflow) specificity	MSCi (outflow) sensitivity	MSCi (outflow) specificity	MSC sensitivity	MSC specificity	Overall model accuracy (inflow and outflow separate)	Overall model accuracy (inflow and outflow combined)
Γ = 0.50										
GhostParser	0.93	0.91	0.88	0.86	0.37	0.95	0.99	1.00	0.79	0.91
BPP	0.85	0.91	0.97	0.57	0.52	0.98	0.07	0.76	0.61	0.71
Γ = 0.30										
GhostParser	0.91	0.95	0.88	0.91	0.44	0.95	0.97	0.99	0.80	0.92
BPP	0.82	0.88	0.90	0.58	0.50	1.00	0.10	0.77	0.58	0.69
Γ = 0.10										
GhostParser	0.67	0.99	0.61	0.81	0.37	0.92	0.98	0.84	0.66	0.80
BPP	0.50	0.92	0.87	0.47	0.52	1.00	0.12	1.00	0.50	0.61
Γ = 0.05										
GhostParser	0.35	1.00	0.41	0.82	0.22	0.96	0.98	0.55	0.50	0.60
BPP	0.38	0.90	0.80	0.39	0.45	0.98	0.05	1.00	0.41	0.53
Γ = 0.01										
GhostParser	0.03	1.00	0.03	0.98	0.02	0.99	0.99	0.06	0.27	0.24

Table 1: Sensitivity and specificity for each introgression model are shown for both BPP and GhostParser under tested introgression probabilities (Γ). BPP was not tested at Γ = 0.01. MSC = multispecies coalescent, MSCi = multispecies coalescent with introgression, MSCig = multispecies coalescent with ghost introgression.

688

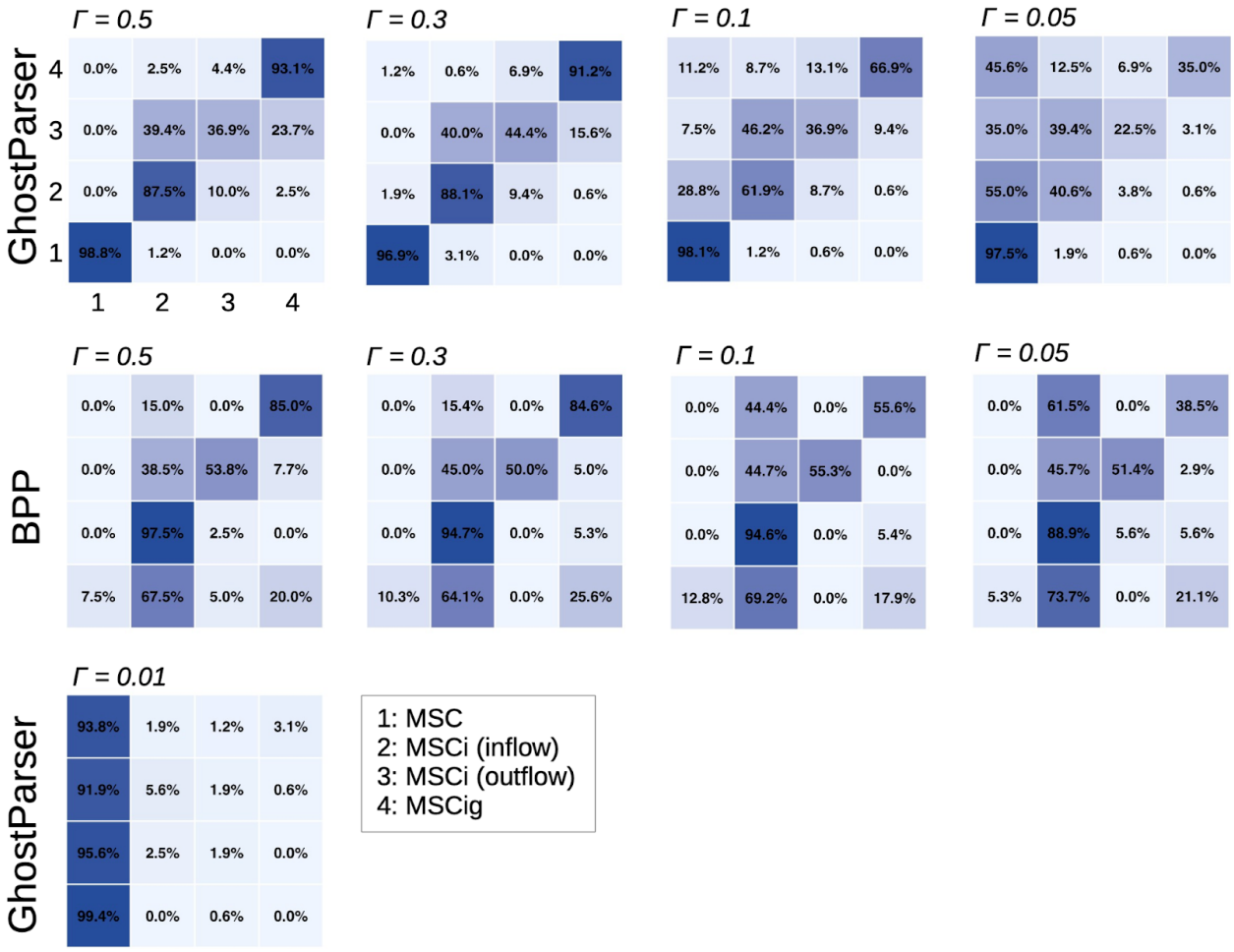

Fig. 7 Performance comparison of GhostParser and BPP on simulated datasets: Confusion matrices show percentage accuracy for each class, where Γ indicates introgression probability. Correct classifications appear along the diagonal, while all off-diagonal entries represent misclassifications. MSC = multispecies coalescent, MSCi = multispecies coalescent with introgression, MSCig = multispecies coalescent with ghost introgression.

Empirical comparisons to BPP

Jaltomata

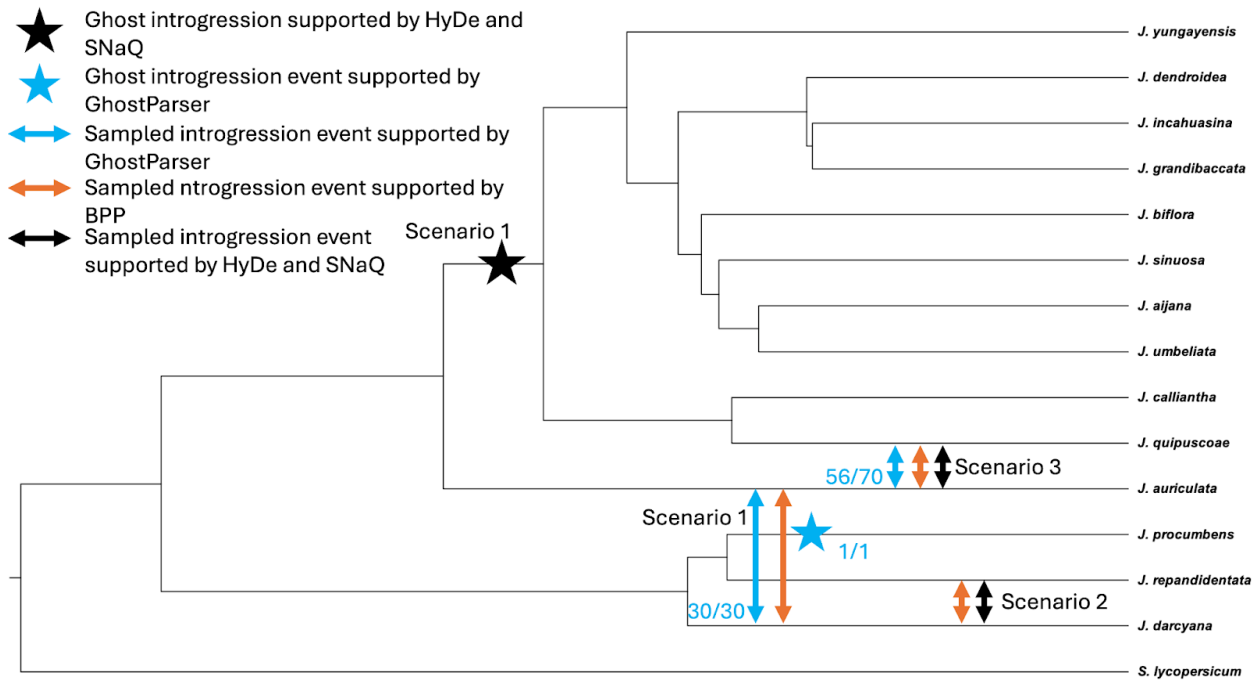

Fig. 8 Introgression within the genus Jaltomata: Scenario 1 is a reticulation event classified as ghost introgression by summary statistic based method HyDe and the network method SNaQ, but as sampled introgression by the full likelihood method BPP (Pang and Zhang 2024) and GhostParser. Scenarios two and three were classified as sampled introgression by HyDe, SNaQ, BPP (Pang and Zhang 2024), while only scenario three was classified as sampled introgression by GhostParser. The ratios represent the proportion of triplets supporting the introgression hypothesis (either ghost or sampled) in GhostParser.

In scenario 1 in the *Jaltomata* tree, which SNaQ and HyDe identified as ghost introgression, but BPP classified as sampled introgression (Pang and Zhang 2024), all thirty triplets tested with GhostParser supported the hypothesis of sampled introgression (**Fig. 8**). GhostParser classified scenario two (1/1 triplets) as ghost introgression, contrary to BPP, HyDe and SNaQ, and classified scenario three (56/70 triplets) as sampled introgression, as did BPP, HyDe and SNaQ. GhostParser classified each sampled introgression event as “inflow”, contrary to BPP which classified the events as “outflow.”

Thuja

In the species triplet ((*T. sutchuensis*, *T. standishi*), *T. plicata*) GhostParser supported the hypothesis of *T. sutcheuensis* being the recipient of ghost introgression, a result consistent with BPP and PhyloNet findings, whereas HyDe inferred only sampled introgression between *T.*

plicata and *T. standishi.*

Heliconius

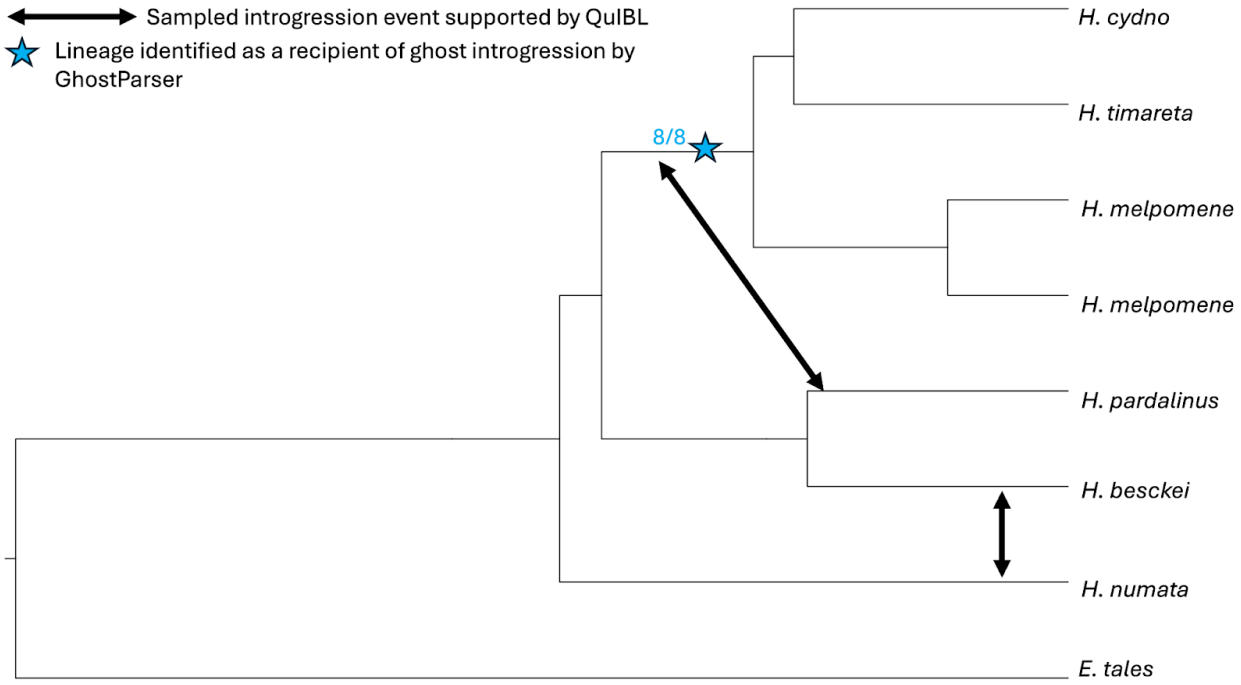

Fig. 9: Introgression within the melpomene clade of Heliconious generated from trees of sliding windows of the Heliconius genome alignment (Edelman et al. 2019). Introgression events detected with QuIBL are shown in black arrows, and ghost introgression detected with GhostParser are shown with blue stars alongside the number of supporting triplets.

GhostParser identified both instances of introgression identified by QuIBL in the melpomene clade of *Heliconius* as ghost introgression, with the *H. cydno*, *H. timareta, H. melpomene* clade identified as the recipient of ghost introgression (**Fig. 9**). However, in all tested triplets, the gene trees supporting the sampled introgression hypothesis (from QuIBL) had a higher count than the species tree topology (Fig. 9), suggesting the species tree hypothesis we used as input for GhostParser (Edelman et al. 2019) may be incorrect.

Drosophila

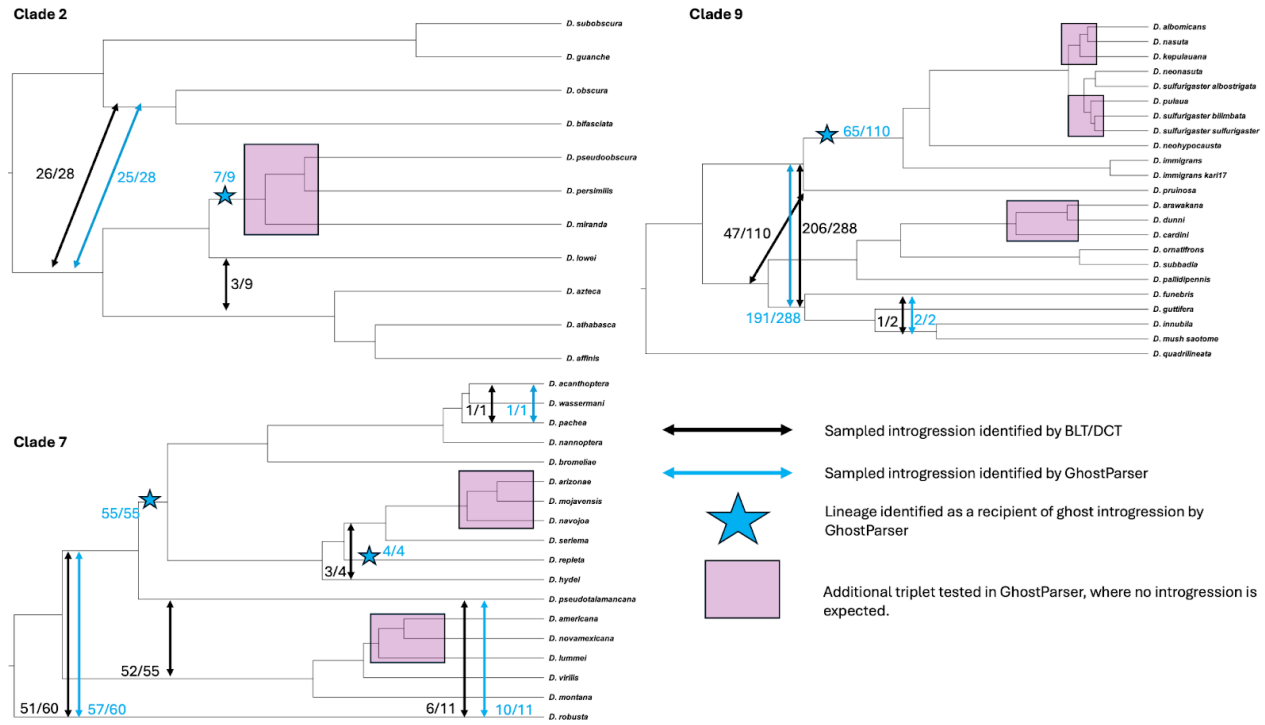

Fig. 10: Introgression across clades 2, 7, and 9 of Drosophila: Previously detected introgression events with BLT/DCT shown in black arrows, with the number of supporting triplets in black. Sampled introgression events detected by GhostParser are shown in blue arrows with the number of supporting triplets in blue, and lineages identified as recipients of ghost introgression are marked with blue stars, with the number of triplets supporting ghost introgression also shown in blue text. Additional clades tested with GhostParser are highlighted in pink. GhostParser did not identify reticulation events in any of these clades. The proportion of triplets supporting the introgression hypotheses from BLT and DCT are shown in black, while the proportion of triplets supporting the GhostParser hypothesis are shown in blue.

One of the sampled introgression events in Clade 2 of *Drosophila* was classified as ghost introgression (7/9 triplets) by GhostParser, while the other gene flow events showed support for sampled introgression (25/28; **Fig. 10**). Two events in Clade 7 were classified as sampled introgression by GhostParser (**Fig. 10**), with the other two being classified as ghost introgression. One of the introgression events in Clade 9 showed mixed support for sampled (60/110 triplets) and ghost (50/110) introgression, while the other two were classified as sampled introgression (**Fig. 10**). Ghostfinder did not identify any other taxa in the species tree which introgressed with the ghost recipients in either Clades 2 or 7. This suggests that the “ghost” lineages were likely unsampled sister groups to Clades 2 and 7 respectively.

Discussion

Towards scalable selection of an appropriate introgression model in the presence of rate variation

Despite the major influence that both sampled and ghost introgression can have on evolutionary inference (Whitney et al. 2006; Pardo-Diaz et al. 2012; Huerta-Sánchez et al. 2014; Bastide et al. 2018; Jones et al. 2018; Taylor and Larson 2019; Ottenburghs 2020b; Gibson et al. 2021; Hibbins and Hahn 2021), no bioinformatic tools exist which can accurately, robustly and in a scalable manner distinguish between these two introgression scenarios from multi-locus phylogenomic datasets (Pang and Zhang, 2024), particularly in the presence of between lineage rate variation (Frankel and Ané 2023; Koppetsch et al. 2024). By considering a novel summary statistic $H(T)$ used by our THT, we successfully identify the presence and absence of ghost and sampled introgression in simulated datasets.

Indeed both simulated and empirical results provide compelling evidence that GhostParser is a reliable approach to estimate both ghost and sampled introgression, even when only one triplet is available for testing, as was the case in the simulated datasets. Not only is the sensitivity of GhostParser to ghost introgression high (>75%) when $\Gamma \geq 0.1$ in our simulations, but GhostParser also rarely misclassifies cases generated under either MSC or MSCi models as ghost introgression (**Table 1**). Nor did GhostParser identify introgression in the tested empirical triplets for which other methodologies did not identify evidence of introgression (**Fig. 10**). GhostParser concurred with BPP in the empirical *Jaltomata* and *Thuja* datasets, even at nodes where other network and summary-statistic based tests differed, with the exception of classifying one reticulation event in *Jaltomata* as ghost introgression (**Fig. 8**). However, the overall accuracy of GhostParser drops when inflow and outflow are considered to be two separate categories, as does the accuracy of the state-of-the-art method BPP (**Table 1**).

BPP exhibited inferior performance in comparison with GhostParser in terms of accuracy criteria metrics (**Table 1**). In particular, BPP produced less accurate results (overall accuracy) than GhostParser, failing to distinguish between simple MSC models with no introgression and

807 MSCi models regardless of Γ, and in distinguishing between inflow and outflow introgression
808 (**Table 1**). We do note that Pang and Zhang's (2024) work did not include a no-introgression
809 scenario in their initial tests of the use of BPP to distinguish between ghost and sampled
810 introgression hypotheses. Furthermore, unlike BPP, GhostParser was highly scalable. It
811 considered each tested triplet in < 20 seconds, compared to the hours, or even days, of real time
812 required by the full-likelihood method employed by BPP. This makes GhostParser more
813 accessible to researchers with more limited computational resources.

814 According to our current understanding of introgression and rate variation, GhostParser
815 succeeds where other heuristic and pseudo-likelihood tests have failed because of its usage of
816 the $H(T)$ statistic in its THT approach. Other branch length tests compare summaries of
817 distances between sister taxa.. For example, The BLT method will compare the distribution of
818 genetic distances between the sister pair BC in G_{dis1} and AC in G_{dis2}; if these distances
819 significantly differ, B and C are assumed to have introgressed (Suvorov et al., 2022A). If, for
820 example, B evolved more rapidly than C, these genetic distances will be skewed mimicking an
821 introgression signal (Frankel and Ané 2023). Likewise, if A introgressed with the ghost lineage X,
822 the proportions of G_{dis1} and G_{dis2} would be significantly different, causing the DCT to infer
823 introgression between B and C (Suvorov et al., 2022A), while the BLT concludes no introgression
824 has occurred. By using the $H(T)$ statistic, GhostParser generates a low false positive rate for
825 introgression detection in the presence of between lineage rate variation allowing reliable
826 inference of sampled and ghost introgression.

827

828 ***Suggested Implementation of GhostParser***

829 GhostParser can be implemented as a stand alone tool to detect introgression, or as a follow up
830 analysis to assess results of prior introgression estimates produced by various methods.
831 GhostParser can be used to test specific hypotheses, and determine if the identified gene flow

events may be the result of ghost introgression, or if introgression has occurred at all. While the sensitivity and accuracy of GhostParser was diminished for simulated scenarios with low introgression probability (i.e. $\Gamma < 0.1$), as compared to larger tested values of introgression strength, this did not appear to hamper its ability to detect ghost and sampled introgression in our sampled empirical systems. Nevertheless, BPP is marginally more sensitive to ghost introgression at $\Gamma = 0.05$, thus the user may want to consider further analysis with BPP if they suspect a false negative result. Under all scenarios of introgression strength ($\Gamma = 0.01, 0.05, 0.10, 0.30, 0.50$), GhostParser remains highly specific in its classification of ghost introgression (**Table 1**). We do caution against relying on GhostParser or BPP to identify the presence of inflow. Accordingly, we did not consider inflow in our empirical dataset analyzed with GhostParser, except in systems where BPP was explicitly used to model the directionality of gene flow. The GhostParser approach distinguishing between ghost and sampled introgression opens the field of reliable and fast introgression detection to those limited by time and computational resources. This will be an important software in introgression detection and systematics.

Data Availability

The ghostparser software, tutorial, and all data for the empirical systems tested are publicly available on github (https://github.com/asuvorovlab/ghostparser.git). The simulated dataset used to test the accuracy of GhostParser, including the gene trees, gene tree alignments, estimated gene trees, and GhostParser output are available on figshare (https://doi.org/10.6084/m9.figshare.29921969).

Acknowledgements

We would like to thank Daniel Schrider for his helpful feedback on this project. All computational work was conducted on the Advanced Research Computing clusters at Virginia Tech.

Appendix: Derivation of gene tree T_{MRCA} expectations under different multispecies coalescent models.

Here, we provide a detailed derivation of three taxon gene tree expectations ($\mathbb{E}[T_{MRCA}]$) for the multispecies coalescent (MSC), multispecies coalescent with sampled bidirectional introgression (MSCi) and multispecies coalescent with unsampled ("ghost") introgression (MSCig) models (**Fig 1 a-c**). Under all these models $\mathbb{E}[T_{MRCA}]$ can be viewed as a sum of tree height expectations multiplied by their corresponding probabilities ω. For instance, in the MSC model, a concordant gene tree can occur in two different ways, where A and B lineages either coalesce in the ancestral population AB or ABC. Each of those two scenarios will have its own probabilities of occurrence ω_1 and ω_2. Also, note that $\omega_1 + \omega_2 = P(G_c)$. Two discordant topologies can only occur in ancestral population ABC with probabilities ω_3 and ω_4. Additionally, for concordant topology where A and B coalesce in population AB the T_{MRCA} expectation is $a = \mathbb{E}_{\theta_{ABC}}[h_{ABC} + T_2]$, whereas for the other concordant topology and both discordant topologies the T_{MRCA} expectation is $b = \mathbb{E}_{\theta_{ABC}}[h_{ABC} + T_2 + T_3]$. Thus:

$$\mathbb{E}[T_{MRCA}] = \omega_1 a + \omega_2 b + \omega_3 b + \omega_4 b.$$

However this model is overparametrized since $\omega_1 = 1 - P^{(2)}{}_{0,AB}$ and $\omega_2 = \omega_3 = \omega_4 = \frac{1}{3}P^{(2)}{}_{0,AB}$, where $P^{(2)}{}_{0,AB} = e^{-\frac{2}{\theta_{AB}}(h_{ABC}-h_{AB})}$. Hence, we can simplify the expectation mixture:

$$\mathbb{E}[T_{MRCA}] = \omega_1 a + \omega_2 b + \omega_2 b + \omega_2 b = \omega_1 a + 3\omega_2 b.$$

Then, gene tree T_{MRCA} expectations for concordant and discordant topologies can be obtained by reweighting (normalizing) each individual mixture component, i.e.

$$\mathbb{E}_{G_c}[T_{MRCA}] = \frac{\omega_1 a + \omega_2 b}{\omega_1 + \omega_2}, \mathbb{E}_{G_{dis1}}[T_{MRCA}] = b, \mathbb{E}_{G_{dis2}}[T_{MRCA}] = b.$$

Similarly, we derive total $\mathbb{E}[T_{\mathrm{MRCA}}]$ for MSCi, where additional outflow and inflow $\Gamma = (\gamma_1, \gamma_2)$ introgression probability parameters are introduced:

$$\begin{aligned}
\mathbb{E}[T_{MRCA}] = {} & (1-\gamma_1)(1-\gamma_2)(\omega_1 a + \omega_2 b) \\
& + \gamma_1(1-\gamma_2)\omega_3 b \\
& + \gamma_2(1-\gamma_1)(\omega_4 c + \omega_5 a + \omega_6 b) \\
& + \gamma_1\gamma_2\omega_7 b, \\
& + (1-\gamma_1)(1-\gamma_2)\omega_8 b \\
& + \gamma_1(1-\gamma_2)(\omega_9 a + \omega_{10} b) \\
& + \gamma_2(1-\gamma_1)(\omega_{11} d + \omega_{12} c + \omega_{13} a + \omega_{14} a + \omega_{15} b) \\
& + \gamma_1\gamma_2\omega_{16} b, \\
& + (1-\gamma_1)(1-\gamma_2)\omega_{17} b \\
& + \gamma_1(1-\gamma_2)\omega_{18} b \\
& + \gamma_2(1-\gamma_1)(\omega_{19} c + \omega_{20} a + \omega_{21} b) \\
& + \gamma_1\gamma_2(\omega_{22} a + \omega_{23} b),
\end{aligned}$$

where $\sum_i (1-\gamma_1)(1-\gamma_2)\omega_i + \sum_j \gamma_1(1-\gamma_2)\omega_j + \sum_l \gamma_2(1-\gamma_1)\omega_l + \sum_m \gamma_1\gamma_2\omega_m = 1$, $\sum_{i=1}^{2}(1-\gamma_1)(1-\gamma_2)\omega_i + \gamma_1(1-\gamma_2)\omega_3 + \sum_{l=4}^{6}\gamma_2(1-\gamma_1)\omega_l + \gamma_1\gamma_2\omega_7 = P(G_c)$, $(1-\gamma_1)(1-\gamma_2)\omega_8 + \sum_{j=9}^{10}\gamma_1(1-\gamma_2)\omega_j + \sum_{l=11}^{15}\gamma_2(1-\gamma_1)\omega_l + \gamma_1\gamma_2\omega_{16} = P(G_{dis1})$ and $(1-\gamma_1)(1-\gamma_2)\omega_{17} + \gamma_1(1-\gamma_2)\omega_{18} + \sum_{l=19}^{21}\gamma_2(1-\gamma_1)\omega_l + \sum_{m=22}^{23}\gamma_1\gamma_2\omega_m = P(G_{dis2})$.

Here we define three probabilities (i) $P^{(3)}{}_{2,AB}$ of observing exactly two coalescences for three lineages in a population AB, (ii) $P^{(3)}{}_{1,AB}$ of exactly one coalescence for three lineages in a population AB and (iii) $P^{(3)}{}_{0,AB}$ of no coalescences for three lineages in population AB (Rosenberg 2002). Also, note that $P^{(3)}{}_{2,AB} + P^{(3)}{}_{1,AB} + P^{(3)}{}_{0,AB} = 1$.

$$P^{(3)}{}_{0,AB} = e^{-3\frac{2}{\theta_{AB}}(h_{ABC} - h_{AB})},$$

$$P^{(3)}_{1,AB} = 1 - \frac{3}{2}e^{-\frac{2}{\theta_{AB}}(h_{ABC}-h_{AB})} + \frac{1}{2}e^{-3\frac{2}{\theta_{AB}}(h_{ABC}-h_{AB})},$$

$$P^{(3)}_{2,AB} = \frac{3}{2}e^{-\frac{2}{\theta_{AB}}(h_{ABC}-h_{AB})} - \frac{3}{2}e^{-3\frac{2}{\theta_{AB}}(h_{ABC}-h_{AB})}.$$

These probabilities that involve coalescence of three branches can be conveniently expressed in terms of $P^{(2)}_{0,AB} = e^{-\frac{2}{\theta_{AB}}(h_{ABC}-h_{AB})}$, i.e.

$$P^{(3)}_{0,AB} = (P^{(2)}_{0,AB})^3,$$

$$P^{(3)}_{1,AB} = 1 - \frac{3}{2}P^{(2)}_{0,AB} + \frac{1}{2}(P^{(2)}_{0,AB})^3,$$

$$P^{(3)}_{2,AB} = \frac{3}{2}P^{(2)}_{0,AB} - \frac{3}{2}(P^{(2)}_{0,AB})^3,$$

$$P^{(2)}_{0,B} = e^{-\frac{2}{\theta_B}(h_{AB}-h_i)},$$

$$P^{(2)}_{0,C} = e^{-\frac{2}{\theta_C}(h_{ABC}-h_i)}.$$

Now, we can establish the equality constraints between different model weights:

$$\omega_1 = \omega_{22} = 1 - P^{(2)}_{0,AB},$$

$$\omega_2 = \omega_8 = \omega_{17} = \frac{1}{3}P^{(2)}_{0,AB},$$

$$\omega_3 = \omega_{10} = \omega_{18} = P^{(2)}_{0,C},$$

$$\omega_4 = \omega_{12} = \omega_{19} = \frac{1}{3}P^{(2)}_{0,B}P^{(3)}_{2,AB},$$

$$\omega_5 = \omega_{13} = \omega_{20} = \frac{1}{3}P^{(2)}_{0,B}P^{(3)}_{1,AB},$$

$$\omega_6 = \omega_{15} = \omega_{21} = \frac{1}{3}P^{(2)}_{0,B}P^{(3)}_{0,AB},$$

$$\omega_7 = \omega_{16} = \omega_{23} = \frac{1}{3}P^{(2)}_{0,AB},$$

$$\omega_9 = 1 - P^{(2)}_{0,C},$$

$$\omega_{11} = (1 - P^{(2)}_{0,B})(1 - P^{(2)}_{0,AB}),$$

$$\omega_{14} = (1 - P^{(2)}_{0,B})P^{(2)}_{0,AB}.$$

The only weights that are not constrained include (ω_9, ω_{11}, ω_{14}) and are unique to discordant topology G_{dis1} mixture component, thus:

$$\mathbb{E}[T_{MRCA}] = (1 - \gamma_1)(1 - \gamma_2)(\omega_1 a + 3\omega_2 b) + \gamma_1(1 - \gamma_2)(\omega_9 a + 3\omega_3 b)$$

$$+ \gamma_2(1 - \gamma_1)(\omega_{11}d + 3\omega_4 c + (3\omega_5 + \omega_{14})a + 3\omega_6 b)$$
$$+ \gamma_1\gamma_2(\omega_1 a + 3\omega_2 b),$$

$$\mathbb{E}_{G_c}[T_{MRCA}] = \frac{(1-\gamma_1)(1-\gamma_2)(\omega_1 a+\omega_2 b)+\gamma_1(1-\gamma_2)\omega_3 b+\gamma_2(1-\gamma_1)(\omega_4 c+\omega_5 a+\omega_6 b)+\gamma_1\gamma_2\omega_7 b}{(1-\gamma_1)(1-\gamma_2)(\omega_1+\omega_2)+\gamma_1(1-\gamma_2)\omega_3+\gamma_2(1-\gamma_1)(\omega_4+\omega_5+\omega_6)+\gamma_1\gamma_2\omega_7},$$

$$\mathbb{E}_{G_{dis1}}[T_{MRCA}] = \frac{(1-\gamma_1)(1-\gamma_2)\omega_2 b+\gamma_1(1-\gamma_2)(\omega_9 a+\omega_3 b)+\gamma_2(1-\gamma_1)(\omega_{11}d+\omega_4 c+\omega_5 a+\omega_{14}a+\omega_6 b)+\gamma_1\gamma_2\omega_7 b}{(1-\gamma_1)(1-\gamma_2)\omega_2+\gamma_1(1-\gamma_2)(\omega_9+\omega_3)+\gamma_2(1-\gamma_1)(\omega_{11}+\omega_4+\omega_5+\omega_{14}+\omega_6)+\gamma_1\gamma_2\omega_7},$$

$$\mathbb{E}_{G_{dis2}}[T_{MRCA}] = \frac{(1-\gamma_1)(1-\gamma_2)\omega_2 b+\gamma_1(1-\gamma_2)\omega_3 b+\gamma_2(1-\gamma_1)(\omega_4 c+\omega_5 a+\omega_6 b)+\gamma_1\gamma_2(\omega_1 a+\omega_7 b)}{(1-\gamma_1)(1-\gamma_2)\omega_2+\gamma_1(1-\gamma_2)\omega_3+\gamma_2(1-\gamma_1)(\omega_4+\omega_5+\omega_6)+\gamma_1\gamma_2(\omega_1+\omega_7)}.$$

Under MSCig model $\mathbb{E}[T_{MRCA}]$ is expressed as follows

$$\mathbb{E}[T_{MRCA}] = (1 - \gamma)(\omega_1 a + \omega_2 b + \omega_3 c + \omega_4 c + \omega_5 d) + \gamma\,\omega_6 d$$
$$+ (1 - \gamma)(\omega_7 b + \omega_8 c + \omega_9 d) + \gamma\,(\omega_{10}c + \omega_{11}d)$$
$$+ (1 - \gamma)(\omega_{12}b + \omega_{13}c + \omega_{14}d) + \gamma\,\omega_{15}d,$$

where $\sum_i (1 - \gamma)\omega_i + \sum_j \gamma\omega_j = 1$, $\sum_{i=1}^{5}(1 - \gamma)\omega_i + \gamma\omega_6 = P(G_c)$, $\sum_{i=7}^{9}(1 - \gamma)\omega_i + \sum_{j=10}^{11}\gamma\omega_j = P(G_{dis_1})$ and $\sum_{i=12}^{14}(1 - \gamma)\omega_i + \gamma\omega_{15} = P(G_{dis_2})$ and coalescence probabilities:

$$P^{(2)}_{0,AB} = e^{-\frac{2}{\theta_{AB}}(h_{ABC}-h_{AB})},$$
$$P^{(2)}_{0,ABC} = e^{-\frac{2}{\theta_{ABC}}(h_{ABCX}-h_{ABC})},$$
$$P^{(3)}_{0,ABC} = (P^{(2)}_{0,ABC})^3,$$
$$P^{(3)}_{1,ABC} = 1 - \frac{3}{2}P^{(2)}_{0,ABC} + \frac{1}{2}(P^{(2)}_{0,ABC})^3,$$
$$P^{(3)}_{2,ABC} = \frac{3}{2}P^{(2)}_{0,ABC} - \frac{3}{2}(P^{(2)}_{0,ABC})^3,$$

$$\omega_1 = (1 - P^{(2)}_{0,AB})(1 - P^{(2)}_{0,ABC}),$$
$$\omega_2 = \omega_7 = \omega_{12} = \frac{1}{3}P^{(2)}_{0,AB}P^{(3)}_{2,ABC},$$
$$\omega_3 = (1 - P^{(2)}_{0,AB})P^{(2)}_{0,ABC},$$
$$\omega_4 = \omega_8 = \omega_{13} = \frac{1}{3}P^{(2)}_{0,AB}\,P^{(3)}_{1,ABC},$$
$$\omega_5 = \omega_9 = \omega_{14} = \frac{1}{3}P^{(2)}_{0,AB}P^{(3)}_{0,ABC},$$

$$\omega_6 = \omega_{11} = \omega_{15} = \frac{1}{3} P^{(3)}_{0,ABC}.$$

Finally, the applying the weight constraints and mixture weight normalization yields:

$$\mathbb{E}[T_{MRCA}] = (1 - \gamma)(\omega_1 a + 3\omega_2 b + (\omega_3 + 3\omega_4) c + 3\omega_5 d) + \gamma(\omega_4 c + 3\omega_6 d),$$

$$\mathbb{E}_{G_c}[T_{MRCA}] = \frac{(1-\gamma)(\omega_1 a + \omega_2 b + \omega_3 c + \omega_4 c + \omega_5 d) + \gamma\,\omega_6 d}{(1-\gamma)(\omega_1 + \omega_2 + \omega_3 + \omega_4 + \omega_5) + \gamma\,\omega_6},$$

$$\mathbb{E}_{G_{dis1}}[T_{MRCA}] = \frac{(1-\gamma)(\omega_2 b + \omega_4 c + \omega_5 d) + \gamma(\omega_{10} c + \omega_6 d)}{(1-\gamma)(\omega_2 + \omega_4 + \omega_5) + \gamma(\omega_{10} + \omega_6)},$$

$$\mathbb{E}_{G_{dis2}}[T_{MRCA}] = \frac{(1-\gamma)(\omega_2 b + \omega_4 c + \omega_5 d) + \gamma\omega_6 d}{(1-\gamma)(\omega_2 + \omega_4 + \omega_5) + \gamma\omega_6}.$$

References

Allman ES, Baños H, Rhodes JA. 2019. NANUQ: a method for inferring species networks from gene trees under the coalescent model. *Algorithms for Molecular Biology* 14:24.

Bastide P, Solís-Lemus C, Kriebel R, William Sparks K, Ané C. 2018. Phylogenetic Comparative Methods on Phylogenetic Networks with Reticulations. *Syst Biol* 67:800–820.

Baumdicker F, Bisschop G, Goldstein D, Gower G, Ragsdale AP, Tsambos G, Zhu S, Eldon B, Ellerman EC, Galloway JG, et al. 2022. Efficient ancestry and mutation simulation with msprime 1.0. *Genetics* 220:iyab229.

Bernal MA, Gaither MR, Simison WB, Rocha LA. 2017. Introgression and selection shaped the evolutionary history of sympatric sister-species of coral reef fishes (genus: Haemulon). *Molecular Ecology* 26:639–652.

Blischak PD, Chifman J, Wolfe AD, Kubatko LS. 2018. HyDe: A Python Package for Genome-Scale Hybridization Detection. *Systematic Biology* 67:821–829.

Chang J-T, Nakamura K, Chao C-T, Luo M-X, Liao P-C. 2023. Ghost introgression facilitates genomic divergence of a sympatric cryptic lineage in Cycas revoluta. *Ecology and Evolution* 13:e10435.

Edelman NB, Frandsen PB, Miyagi M, Clavijo B, Davey J, Dikow RB, García-Accinelli G, Van Belleghem SM, Patterson N, Neafsey DE, et al. 2019. Genomic architecture and introgression shape a butterfly radiation. *Science* 366:594–599.

Ewens WJ. 2004. Mathematical Population Genetics. New York, NY: Springer Available from: http://link.springer.com/10.1007/978-0-387-21822-9

Flouri T, Jiao X, Rannala B, Yang Z. 2020a. A Bayesian Implementation of the Multispecies Coalescent Model with Introgression for Phylogenomic Analysis. *Molecular Biology and Evolution* 37:1211–1223.

Flouri T, Jiao X, Rannala B, Yang Z. 2020b. A Bayesian Implementation of the Multispecies Coalescent Model with Introgression for Phylogenomic Analysis. *Molecular Biology and Evolution* 37:1211–1223.

Frankel LE, Ané C. 2023. Summary Tests of Introgression Are Highly Sensitive to Rate Variation Across Lineages. *Systematic Biology* 72:1357–1369.

Gibson MJ, Torres M de L, Brandvain Y, Moyle LC. 2021. Introgression shapes fruit color convergence in invasive Galápagos tomato. *eLife* 10:e64165.

Gokcumen O. 2020. Archaic hominin introgression into modern human genomes. *Am J Phys Anthropol* 171 Suppl 70:60–73.

Green RE, Krause J, Briggs AW, Maricic T, Stenzel U, Kircher M, Patterson N, Li H, Zhai W, Fritz MH-Y, et al. 2010. A Draft Sequence of the Neandertal Genome. *Science* 328:710–722.

Hahn MW, Hibbins MS. 2019. A Three-Sample Test for Introgression. *Mol Biol Evol* 36:2878–2882.

Hallström B, Janke A. 2010. Mammalian evolution may not be strictly bifurcating. *Molecular biology and evolution* 27:2804–2816.

Hasegawa M, Kishino H, Yano T. 1985. Dating of the human-ape splitting by a molecular clock of mitochondrial DNA. *J Mol Evol* 22:160–174.

Hey J, Chung Y, Sethuraman A, Lachance J, Tishkoff S, Sousa VC, Wang Y. 2018. Phylogeny Estimation by Integration over Isolation with Migration Models. *Molecular Biology and Evolution* 35:2805–2818.

Hibbins MS, Hahn MW. 2021. The effects of introgression across thousands of quantitative traits revealed by gene expression in wild tomatoes. *PLoS Genet* 17:e1009892.

Hibbins MS, Hahn MW. 2022. Phylogenomic approaches to detecting and characterizing introgression.Turelli M, editor. *Genetics* 220:iyab173.

Hudson RR. 2002. Generating samples under a Wright–Fisher neutral model of genetic variation. *Bioinformatics* 18:337–338.

Huerta-Cepas J, Serra F, Bork P. 2016. ETE 3: Reconstruction, Analysis, and Visualization of Phylogenomic Data. *Mol Biol Evol* 33:1635–1638.

Huerta-Sánchez E, Jin X, Asan, Bianba Z, Peter BM, Vinckenbosch N, Liang Y, Yi X, He M, Somel M, et al. 2014. Altitude adaptation in Tibetans caused by introgression of Denisovan-like DNA. *Nature* 512:194–197.

Huson DH, Bryant D. 2006. Application of Phylogenetic Networks in Evolutionary Studies. *Molecular Biology and Evolution* 23:254–267.

Jiao X, Flouri T, Yang Z. 2021. Multispecies coalescent and its applications to infer species phylogenies and cross-species gene flow. *National Science Review* 8:nwab127.

Jones MR, Mills LS, Alves PC, Callahan CM, Alves JM, Lafferty DJR, Jiggins FM, Jensen JD, Melo-Ferreira J, Good JM. 2018. Adaptive introgression underlies polymorphic seasonal camouflage in snowshoe hares. *Science* 360:1355–1358.

Junier T. 2024. tjunier/newick_utils. Available from: https://github.com/tjunier/newick_utils

Katoh K, Standley DM. 2013. MAFFT Multiple Sequence Alignment Software Version 7: Improvements in Performance and Usability. *Molecular Biology and Evolution* 30:772–780.

King MC, Rosenberg NA. 2021. A simple derivation of the mean of the Sackin index of tree balance under the uniform model on rooted binary labeled trees. *Mathematical Biosciences* 342:108688.

Koller D, Wendt FR, Pathak GA, De Lillo A, De Angelis F, Cabrera-Mendoza B, Tucci S, Polimanti R. 2022. Denisovan and Neanderthal archaic introgression differentially impacted the genetics of complex traits in modern populations. *BMC Biology* 20:249.

Koppetsch T, Malinsky M, Matschiner M. 2024. Towards reliable detection of introgression in the presence of among-species rate variation. :2023.05.21.541635. Available from: https://www.biorxiv.org/content/10.1101/2023.05.21.541635v2

Kumar V, Lammers F, Bidon T, Pfenninger M, Kolter L, Nilsson MA, Janke A. 2017. The evolutionary history of bears is characterized by gene flow across species. *Sci Rep* 7:46487.

Leduc-Robert G, Maddison WP. 2018. Phylogeny with introgression in Habronattus jumping spiders (Araneae: Salticidae). *BMC Evol Biol* 18:24.

Li J, Zhang Y, Ruhsam M, Milne RI, Wang Y, Wu D, Jia S, Tao T, Mao K. 2022. Seeing through the hedge: Phylogenomics of Thuja (Cupressaceae) reveals prominent incomplete lineage sorting and ancient introgression for Tertiary relict flora. *Cladistics* 38:187–203.

Ly-Trong N, Naser-Khdour S, Lanfear R, Minh BQ. 2022. AliSim: A Fast and Versatile Phylogenetic Sequence Simulator for the Genomic Era. *Molecular Biology and Evolution* 39:msac092.

Maddison W. 1997. Gene Trees in Species Trees. *Systematic Biology* 46:523–536.

Malinsky M, Matschiner M, Svardal H. 2021. Dsuite - Fast D-statistics and related admixture evidence from VCF files. *Molecular Ecology Resources* 21:584–595.

Mallet J. 2005. Hybridization as an invasion of the genome. *Trends in Ecology & Evolution* 20:229–237.

McArthur E, Rinker DC, Capra JA. 2021. Quantifying the contribution of Neanderthal introgression to the heritability of complex traits. *Nat Commun* 12:4481.

Miller RJ, Mione T, Phan H-L, Olmstead RG. 2011. Color by Numbers: Nuclear Gene Phylogeny of Jaltomata (Solanaceae), Sister Genus to Solanum, Supports Three Clades Differing in Fruit Color. *Systematic Botany* 36:153–162.

Minh BQ, Schmidt HA, Chernomor O, Schrempf D, Woodhams MD, von Haeseler A, Lanfear R. 2020. IQ-TREE 2: New Models and Efficient Methods for Phylogenetic Inference in the Genomic Era. *Molecular Biology and Evolution* 37:1530–1534.

Naser-Khdour S, Minh BQ, Lanfear R. 2025. The Influence of Model Violation on Phylogenetic Inference: A Simulation Study. :2021.09.22.461455. Available from: https://www.biorxiv.org/content/10.1101/2021.09.22.461455v2

Ogden TH, Rosenberg MS. 2006. Multiple sequence alignment accuracy and phylogenetic inference. *Syst Biol* 55:314–328.

Ottenburghs J. 2020a. Ghost Introgression: Spooky Gene Flow in the Distant Past. *BioEssays* 42:2000012.

Ottenburghs J. 2020b. Ghost Introgression: Spooky Gene Flow in the Distant Past. *BioEssays* 42:2000012.

Pamilo P, Nei M. 1988. Relationships between gene trees and species trees. *Molecular Biology and Evolution* 5:568–583.

Pang X-X, Zhang D-Y. 2023. Impact of Ghost Introgression on Coalescent-Based Species Tree Inference and Estimation of Divergence Time. *Systematic Biology* 72:35–49.

Pang X-X, Zhang D-Y. 2024. Detection of Ghost Introgression Requires Exploiting Topological and Branch Length Information. *Systematic Biology* 73:207–222.

Pardo-Diaz C, Salazar C, Baxter SW, Merot C, Figueiredo-Ready W, Joron M, McMillan WO, Jiggins CD. 2012. Adaptive Introgression across Species Boundaries in Heliconius Butterflies. *PLOS Genetics* 8:e1002752.

Pease JB, Hahn MW. 2015. Detection and Polarization of Introgression in a Five-Taxon Phylogeny. *Systematic Biology* 64:651–662.

Pfeifer B, Kapan DD, Herzog SA. 2024. Detection and quantification of introgression using Bayesian inference based on conjugate priors. *Bioinformatics* 40:btae642.

Phillips MJ, Delsuc F, Penny D. 2004. Genome-Scale Phylogeny and the Detection of Systematic Biases. *Mol Biol Evol* 21:1455–1458.

Qian Y, Meng M, Zhou C, Liu H, Jiang H, Xu Y, Chen W, Ding Z, Liu Y, Gong X, et al. 2023. The Role of Introgression During the Radiation of Endemic Fishes Adapted to Living at Extreme Altitudes in the Tibetan Plateau. *Molecular Biology and Evolution* 40:msad129.

R Core Team. 2021. R: A language and environment for statistical computing.

Rannala B, Yang Z. 2003. Bayes Estimation of Species Divergence Times and Ancestral Population Sizes Using DNA Sequences From Multiple Loci. *Genetics* 164:1645–1656.

Rosenberg NA. 2002. The Probability of Topological Concordance of Gene Trees and Species Trees. *Theoretical Population Biology* 61:225–247.

Singhal S, Derryberry GE, Bravo GA, Derryberry EP, Brumfield RT, Harvey MG. 2021. The dynamics of introgression across an avian radiation. *Evolution Letters* 5:568–581.

Solís-Lemus C, Ané C. 2016. Inferring Phylogenetic Networks with Maximum Pseudolikelihood under Incomplete Lineage Sorting. *PLOS Genetics* 12:e1005896.

Solís-Lemus C, Bastide P, Ané C. 2017. PhyloNetworks: A Package for Phylogenetic Networks. *Molecular Biology and Evolution* 34:3292–3298.

Stull GW, Pham KK, Soltis PS, Soltis DE. 2023. Deep reticulation: the long legacy of hybridization in vascular plant evolution. *The Plant Journal* 114:743–766.

Suvorov A, Kim BY, Wang J, Armstrong EE, Peede D, D'Agostino ERR, Price DK, Waddell P, Lang M, Courtier-Orgogozo V, et al. 2022. Widespread introgression across a phylogeny of 155 Drosophila genomes. *Curr Biol* 32:111-123.e5.

Suvorov A, Scornavacca C, Fujimoto MS, Bodily P, Clement M, Crandall KA, Whiting MF, Schrider DR, Bybee SM. 2021. Deep Ancestral Introgression Shapes Evolutionary History of Dragonflies and Damselflies. *Systematic Biology*:syab063.

Taylor SA, Larson EL. 2019. Insights from genomes into the evolutionary importance and prevalence of hybridization in nature. *Nat Ecol Evol* 3:170–177.

Teixeira JC, Cooper A. 2019. Using hominin introgression to trace modern human dispersals. *Proceedings of the National Academy of Sciences* 116:15327–15332.

Thawornwattana Y, Seixas FA, Yang Z, Mallet J. 2023. Major patterns in the introgression history of Heliconius butterflies. :2023.06.21.545923. Available from: https://www.biorxiv.org/content/10.1101/2023.06.21.545923v2

Tricou T, Tannier E, de Vienne DM. 2022. Ghost Lineages Highly Influence the Interpretation of Introgression Tests. *Systematic Biology* 71:1147–1158.

Tricou T, Tannier E, Vienne DM de. 2022. Ghost lineages can invalidate or even reverse findings regarding gene flow. *PLOS Biology* 20:e3001776.

Wakeley J. 2009. Coalescent Theory: An Introduction. Greenwood Village: W. H. Freeman

Wen D, Nakhleh L. 2018. Coestimating Reticulate Phylogenies and Gene Trees from Multilocus Sequence Data. *Systematic Biology* 67:439–457.

Whitney KD, Randell RA, Rieseberg LH. 2006. Adaptive Introgression of Herbivore Resistance Traits in the Weedy Sunflower Helianthus annuus. *The American Naturalist* 167:794–807.

Wong KM, Suchard MA, Huelsenbeck JP. 2008. Alignment uncertainty and genomic analysis. *Science* 319:473–476.

Wu D-D, Ding X-D, Wang S, Wójcik JM, Zhang Y, Tokarska M, Li Y, Wang M-S, Faruque O, Nielsen R, et al. 2018. Pervasive introgression facilitated domestication and adaptation in the Bos species complex. *Nat Ecol Evol* 2:1139–1145.

Yang Z. 1994. Maximum likelihood phylogenetic estimation from DNA sequences with variable rates over sites: Approximate methods. *J Mol Evol* 39:306–314.

Yang Z. 1996. Among-site rate variation and its impact on phylogenetic analyses. *Trends in Ecology & Evolution* 11:367–372.

Yang Z. 2015. The BPP program for species tree estimation and species delimitation. *Current Zoology* 61:854–865.

Yu Y, Dong J, Liu KJ, Nakhleh L. 2014a. Maximum likelihood inference of reticulate evolutionary histories. *Proceedings of the National Academy of Sciences* 111:16448–16453.

Yu Y, Dong J, Liu KJ, Nakhleh L. 2014b. Maximum likelihood inference of reticulate evolutionary histories. *Proc Natl Acad Sci U S A* 111:16448–16453.

Yu Y, Dong J, Liu KJ, Nakhleh L. 2014c. Maximum likelihood inference of reticulate evolutionary histories. *Proceedings of the National Academy of Sciences* 111:16448–16453.

Yu Y, Nakhleh L. 2015. A maximum pseudo-likelihood approach for phylogenetic networks. *BMC Genomics* 16:S10.

Zhang C, Ogilvie HA, Drummond AJ, Stadler T. 2018. Bayesian Inference of Species Networks from Multilocus Sequence Data. *Molecular Biology and Evolution* 35:504–517.

Zhang D, Tang L, Cheng Y, Hao Y, Xiong Y, Song G, Qu Y, Rheindt FE, Alström P, Jia C, et al. 2019. “Ghost Introgression” As a Cause of Deep Mitochondrial Divergence in a Bird Species Complex. *Molecular Biology and Evolution* 36:2375–2386.

Zhang W-P, Ding Y-M, Cao Y, Li P, Yang Y, Pang X-X, Bai W-N, Zhang D-Y. 2024. Uncovering ghost introgression through genomic analysis of a distinct eastern Asian hickory species. *The Plant Journal* 119:1386–1399.

Zheng Y, Janke A. 2018. Gene flow analysis method, the D-statistic, is robust in a wide parameter space. *BMC Bioinformatics* 19:10.

Zhu S, Degnan JH. 2017. Displayed Trees Do Not Determine Distinguishability Under the Network Multispecies Coalescent. *Syst Biol* 66:283–298.